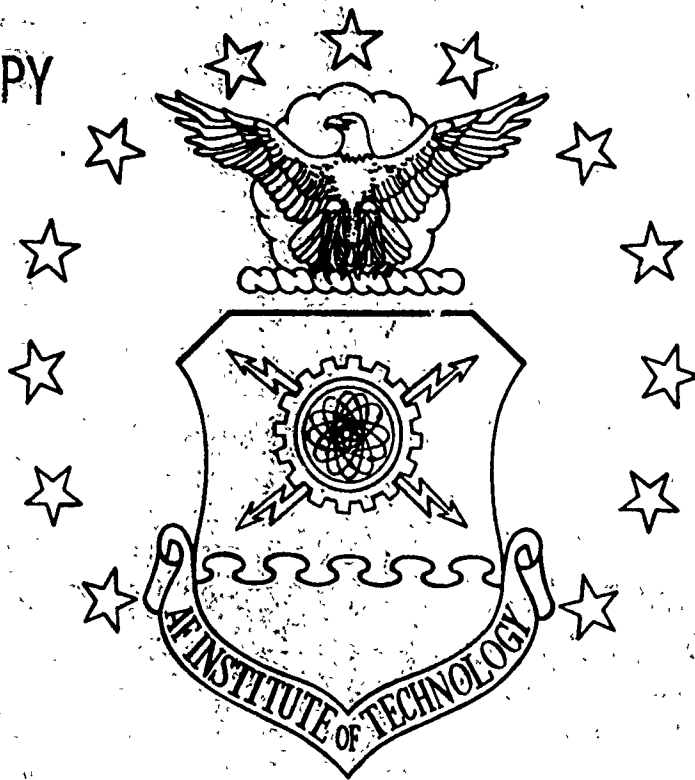


1

DTIC FILE COPY

AD-A230 514



DTIC  
ELECTE  
JAN 07 1991  
S B D

Pulse Compression for Aerosol Ranging  
With Coherent Pulse-Doppler  
Lidar Systems

THESIS

Jerry L. Rogers  
Captain, USAF

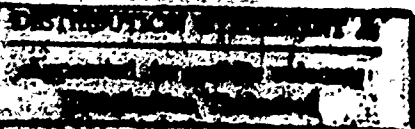
AFIT/GE/ENG/90D-52

DEPARTMENT OF THE AIR FORCE  
AIR UNIVERSITY

**AIR FORCE INSTITUTE OF TECHNOLOGY**

Wright-Patterson Air Force Base, Ohio

91 1 3 132



AFIT/GE/ENG/90D-52

Pulse Compression for Aerosol Ranging  
With Coherent Pulse-Doppler  
Lidar Systems

THESIS

Jerry L. Rogers  
Captain, USAF

AFIT/GE/ENG/90D-52

DTIC  
ELECTE  
JAN 07 1991  
S B D

Approved for public release; distribution unlimited

AFIT/GE/ENG/90D-52

Pulse Compression for Aerosol Ranging With Coherent  
Pulse-Doppler Lidar Systems

THESIS

Presented to the Faculty of the School of Engineering  
of the Air Force Institute of Technology  
Air University  
In Partial Fulfillment of the  
Requirements for the Degree of  
Master of Science in Electrical Engineering

Jerry L. Rogers, B.S.  
Captain, USAF

December 1990

Approved for public release; distribution unlimited

## *Acknowledgments*

I want to thank my thesis advisor Capt. Byron M. Welsh for his many hours of patient assistance and encouragement during this thesis project. I also want to thank Lt Col. David E. Meer for his help and Dr Paul McManamon for his recommendation of this thesis topic for AFIT research.

I am grateful to my christian friends who prayed for my success. I am especially grateful to my wife Rita who diligently supported me every way she possibly could throughout the thesis effort. And finally, I thank the Lord for answered prayer; otherwise, I could not have completed this thesis.

Jerry L. Rogers

<b>Accession For</b>	
NTIS GRA&I	<input checked="checked" type="checkbox"/>
DTIC TAB	<input type="checkbox"/>
Unannounced	<input type="checkbox"/>
Justification	
By _____	
Distribution/	
Availability Codes	
Dist	Avail and/or Special
A-1	



## *Table of Contents*

	Page
Acknowledgments . . . . .	ii
Table of Contents . . . . .	iii
List of Figures . . . . .	v
List of Tables . . . . .	vi
Abstract . . . . .	vii
I. Introduction . . . . .	1
1.1 Background . . . . .	1
1.2 Problem . . . . .	1
1.3 Summary of Current Knowledge . . . . .	2
1.4 Assumptions . . . . .	3
1.5 General Approach and Presentation . . . . .	4
II. A Review of Lidar Developments . . . . .	5
2.1 Historical Development of Lidar Systems . . . . .	5
2.2 Lidar System Description . . . . .	7
2.3 Lidar Theory . . . . .	11
2.4 Lidar Signal Processing . . . . .	13
III. Theory and Methods . . . . .	20
3.1 Introduction . . . . .	20
3.2 Matched-Filter Theory . . . . .	20
3.3 Radar Resolution . . . . .	28

	Page
3.4 Target Model . . . . .	37
3.5 Conventional Radar Receiver . . . . .	46
IV. Findings and Observations . . . . .	50
4.1 Introduction . . . . .	50
4.2 Class 1 Radar Signals . . . . .	52
4.3 Class 2 Radar Signals . . . . .	56
4.4 Class 3 Radar Signals . . . . .	75
4.5 Class 4 Radar Signals . . . . .	80
V. Conclusions and Recommendations . . . . .	87
5.1 Conclusions . . . . .	87
5.2 Recommendations . . . . .	88
Appendix A. Derivation of the MFSLR Response . . . . .	89
Bibliography . . . . .	94
Vita . . . . .	97

## *List of Figures*

Figure	Page
1. Simplified Block Diagram of a Coherent Pulsed-Doppler Lidar . . . .	8
2. Complex Demodulator . . . . .	15
3. Matched-Filter, Square-Law Receiver . . . . .	25
4. Contour Plot of a Class 1 Ambiguity Function (Long Pulse) . . . .	54
5. Contour Plot of a Class 1 Ambiguity Function (Short Pulse) . . . .	54
6. Amplitude (a) and Frequency (b) of the Transmitted Chirp Pulse . .	59
7. Contour Plot of a Class 2 Ambiguity Function . . . . .	62
8. Combined Contour Plots of the Scattering and Ambiguity Functions	72
9. Class 3 Ambiguity Function (a) and Contour Plot (b) . . . . .	77
10. Periodic Pulse Train . . . . .	80
11. Contour Plot of a Class 4 Ambiguity Function . . . . .	82
12. Clear Area about the Central Spike . . . . .	85

## *List of Tables*

Table	Page
1. Ambiguity Function Parameters . . . . .	51



*Abstract*

This thesis provides a thorough review of conventional matched-filter radar theory as it applies to aerosol sensing lidar. Basic matched-filter radar theory and the complex, dense aerosol target model eventually lead to a general derivation of the matched-filter radar receiver response to a dense aerosol target environment. The matched-filter response is obtained in terms of a two dimensional convolution of the target scattering function and the radar ambiguity function. The range and radial velocity resolution of various radar signals were compared using the matched-filter radar receiver and scattering function models. Pulse compression radar signals were compared to the simple radar pulses currently in use with existing lidar systems, and in each case, the pulse compression radar signal did not provide a significant improvement in combined range and radial velocity resolution.

# Pulse Compression for Aerosol Ranging With Coherent Pulse-Doppler Lidar Systems

## *I. Introduction*

### *1.1 Background*

Rapid advances in coherent laser pulse-Doppler radar, commonly known as coherent lidar, have resulted in numerous wind sensing applications such as measurement of wind velocity profiles of severe storms, clear air turbulence (CAT), wind shear, and aircraft wake vortices. Some of these applications, such as aircraft wake vortex detection and wind shear detection, require range resolutions which exceed the capabilities of current lidar systems. Extending classical pulse compression techniques originally developed for conventional radio frequency radar to lidar systems was believed to offer the possibility of improving the combined range and velocity resolution in comparison to current lidar systems which employ simple unmodulated radar pulses.

### *1.2 Problem*

Present "state of the art" lidar systems for wind sensing with a required velocity resolution of approximately 1 m/s are limited in range resolution to approximately 200 m. The objective of this thesis was to research classical pulse compression techniques to determine their potential for improving the combined range and radial velocity resolution of lidar systems. Four basic classes of radar signal were identified. The resolution in combined range and radial velocity for each class of radar signal was determined in terms of the conventional matched-filter radar receiver response to a dense aerosol target environment. The resolution performance for each class of

pulse compression radar signals was thoroughly reviewed and compared to the simple unmodulated radar pulse. The thesis research showed that for a dense aerosol target environment, pulse compression radar signals do not provide improved resolution in combined range and radial velocity in comparison to the simple unmodulated radar signals currently in use with existing lidar systems.

### *1.3 Summary of Current Knowledge*

Lidar systems have become a powerful tool for the measurement of radial wind velocities with numerous wind sensing applications. Extensive research efforts which began in the late 1960s and have continued to the present have resulted in lidar systems with  $CO_2$  continuous wave (CW) transmitters which are amplitude modulated to obtain pulse energies up to 1J with pulse repetition frequencies (PRF) up to 50 Hz. A typical system operating with a  $CO_2$  wavelength of 10  $\mu m$  and with a pulse duration of 1  $\mu s$  can attain a radial velocity resolution of approximately 1 m/s and a radial range resolution of approximately 150–300 m (24). These systems employ optical heterodyne detection which requires a monochromatic CW laser source which is spatially and temporally coherent. The coherence time of the laser transmitter must be greater than the coherence time of the received signal which is determined by atmospheric conditions. The atmosphere is modeled as a diffuse target which consists of a large number of very small aerosol particles such as dust and water droplets. When a pulse of coherent laser energy is transmitted to the atmosphere, the pulse irradiates a volume of air (defined by the beam width and pulse duration) which consists of a large number of these aerosols. According to Mie theory, the backscattered radiation of the received signal is due primarily to suspended aerosols with diameters within one order of magnitude of the laser transmitter wavelength (18). For example, with a 10  $\mu m$  wavelength transmitter, the backscattered radiation is due to aerosols with diameters of approximately 1-3  $\mu m$  (24, 18). Doppler shift measurements of the backscattered optical signal as a function of time result in

range-resolved measurements of radial (line of sight) velocity.

The optical signal is heterodyned to an electrical signal where conventional Doppler signal processors originally developed for millimeter-wave radar are employed. The received optical signal backscattered from the range resolved volume of aerosol particles may be processed to obtain the velocity mean and velocity standard deviation using either time domain, pulse-pair processing techniques or frequency domain, fast fourier transform (FFT) techniques. The most common signal processing approach requires a complex receiver structure of in-phase and quadrature components to determine the correct target velocity direction relative to the lidar followed by transient digitizers and a pulse-pair or spectral processor.

#### *1.4 Assumptions*

A considerable degree of research concerning all aspects of lidar wind sensing has occurred over the past two decades, and models for atmospheric effects and photodetector quantum noise effects have been rigorously developed. Atmospheric models to account for attenuation, speckle, and refractive turbulence are assumed adequate for this research effort. Considerable agreement found in the literature indicates the validity of these models. The net effect of the atmospheric models is a received optical signal which is statistically modeled as a time varying Rayleigh phasor with a Rayleigh-distributed amplitude and a uniformly-distributed phase. The noise current of the quantum noise limited photodetector is statistically modeled as additive white Gaussian noise over the narrow bandwidth of the detector, and the photodetector output current due to the received optical signal is modeled by a narrowband Gaussian random process (24). Errors which may arise from these statistical models or simplifications of the models are accounted for in the analysis as necessary.

In addition to assumptions related to the atmospheric and photodetector statistical models, two additional assumptions are made. The first assumption is based

on Biernson and Lucy's comparison between coherent and direct detection lidar performance which shows that for low signal to noise ratio ( $SNR \leq 1$ ) coherent (heterodyne) detection provides superior detector output SNR performance (4). Therefore, since low SNR is prevalent in wind sensing applications, the analysis will be based only on a heterodyne detection model. The second assumption is based on a review of current lidar transmitters which indicates that  $CO_2$  lidar transmitters operating at 9-12  $\mu m$  wavelengths represent the most mature transmitter technology available for lidar today. Therefore, the analysis will be based only on a  $CO_2$  transmitter model which operates with a wavelength of 9-12  $\mu m$ .

### *1.5 General Approach and Presentation*

Results of this thesis research provide a thorough review of conventional matched-filter radar theory as it applies to an aerosol sensing lidar. Chapter two provides an historical perspective of lidar development along with a brief discussion of current lidar systems and signal processing techniques. Chapter 3 provides a discussion of the basic theory of conventional matched-filter radar receivers, the complex aerosol target model, and the matched-filter radar receiver response to the aerosol target model. In Chapter 4, each of the four basic classes of radar signal are evaluated in terms of their resolution performance in a dense aerosol target environment.

## *II. A Review of Lidar Developments*

Coherent Lidar systems have become a powerful tool for the measurement of radial wind velocities with numerous wind sensing applications. This chapter provides a basic overview of coherent lidar technological and theoretical developments occurring over the past two decades. The chapter begins with a discussion of lidar historical developments, followed by a simplified lidar system description, a brief discussion of lidar theory, and finally, a discussion of lidar signal processing techniques.

### *2.1 Historical Development of Lidar Systems*

In 1980, Bilbro of the NASA Marshall Space Flight Center (MSFC) provided a detailed overview of the historical developments of atmospheric laser Doppler velocimetry which occurred from 1964 to 1980 (6). According to Bilbro, laser Doppler velocimetry theory based on the measurement of the mean frequency of a backscattered target frequency spectrum was first described in 1964. During the early 1970s, the first demonstrated measurements of atmospheric wind velocity occurred using continuous wave (CW) carbon dioxide  $CO_2$  laser systems with operating ranges of approximately 200 m (6, 22). These initial  $CO_2$  CW laser systems were used in a variety of applications in wind sensing such as measuring the wind velocity profiles of wind shear, dust devils, tornadoes, and aircraft wake vortices (6, 22, 32, 17).

During the 1970s and soon after CW systems were designed, the desire to measure clear air turbulence (CAT) motivated the development of coherent pulsed-Doppler lidar systems (6, 24). These systems offered a tenfold increase in range performance. The first air-borne pulsed lidar system was built for NASA/MSFC and employed a master oscillator power amplifier (MOPA) transmitter configuration capable of attaining pulse energies up to 30 mJ and operating ranges up to 6 km (5, 7). The system was later upgraded with the capability of generating two-dimensional wind fields horizontal to the aircraft. The technique for generating these

two-dimensional wind profiles was based on the measurements of wind velocity at the same location from two directions. This upgraded airborne lidar system was flown on the NASA CV-990 during several studies in the early 1980s which successfully measured two-dimensional wind profiles surrounding severe storms (5, 7).

According to Menzies and Hardesty, the development of pulsed transversely-excited atmospheric pressure (TEA)  $CO_2$  laser transmitters was a major milestone of Doppler lidar technological development, and in 1981 the National Oceanic Atmospheric Administration (NOAA) began using the first pulsed TEA  $CO_2$  system to measure atmospheric wind velocities (24). This TEA laser system produced a pulse energy of 100 mJ with a pulse repetition frequency (PRF) of 10 Hz. In a continuing effort to meet the pulse energy requirements of a space-based lidar system, the NOAA Wave Propagation Lab (WPL) later upgraded their hybrid TEA laser transmitter lidar system with an injection-locked TEA laser capable of 1 J pulse energies with a maximum PRF of 50 Hz (13). The NOAA system with the injection controlled TEA transmitter and velocity azimuth display (VAD) scanning techniques to generate three-dimensional wind velocity profiles with color graphics displays represents a "state of the art" lidar system which has been used in numerous wind sensing studies (24).

A major application and motivation for the development of lidar technology has been the concept of an earth orbiting lidar system to generate global three-dimensional wind velocity profiles (24, 10). Numerous feasibility studies, preliminary design specifications, and advances in coherent pulse Doppler lidar technology during the past decade have resulted in a baseline lidar system called the Laser Atmospheric Wind Sounder (LAWS) which is scheduled to become part of NASA's Earth Orbiting System (EOS) in the late 1990s (23, 27, 40). The baseline LAWS system design specifications include a  $CO_2$  laser transmitter operating at a wavelength of  $9.11 \mu m$  with  $3 \mu s$  pulse duration, 10 J pulse energy, and a PRF of up to 10 Hz (24, 10). More recent developments in solid-state laser transmitters for pulsed lidar may result

in a solid-state coherent lidar implementation for LAWS (10, 2, 9). For example, Coherent Technologies Inc. has recently developed and demonstrated a partially solid-state Nd:YAG laser transmitter design (19). Rapid advances in lidar technology have resulted in accurate and reliable coherent pulsed-Doppler lidar systems for three-dimensional wind field measurements with the eventual goal of a space-based lidar system generating global three-dimensional wind velocity profiles.

## *2.2 Lidar System Description*

Several authors have described the theory of coherent laser pulsed-Doppler radar developed more than two decades ago (4, 1). The simplified block diagram of Figure 1 illustrates a typical coherent lidar system employing a MOPA configuration. A signal trace through the various components of Figure 1 will simplify the system description.

Within the MOPA configuration, the spatially coherent, monochromatic CW optical or infrared output beam is amplitude modulated and power amplified to form an optical pulse train signal with a carrier frequency equal to the frequency of the master oscillator. The optical signal is transmitted through the transmit/receive optical duplexer to the telescope and possibly through a scanning mirror to the target which in this application is the aerosols suspended within the atmosphere. The switching electronics of the optical duplexer establishes the time measurements for range gating and protects the detector from the high transmission intensities. In a monostatic radar configuration as illustrated in Figure 1, the same telescope receives the optical signal backscattered from the target. The velocity of the target will cause a shift of the mean frequency of the received signal frequency spectrum according to the well known Doppler equation:

$$F_d = 2V_r/\lambda \quad (1)$$



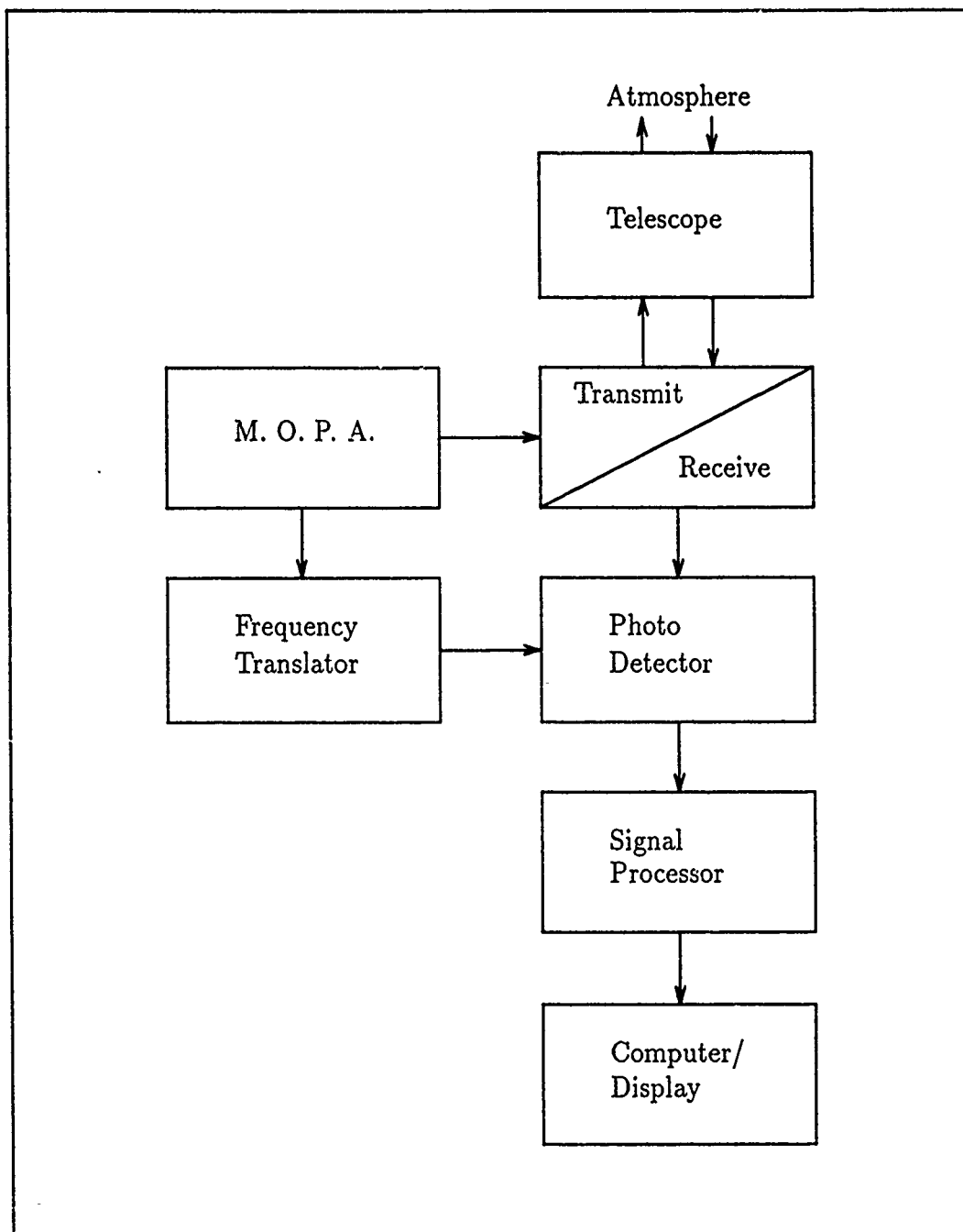


Figure 1. Simplified Block Diagram of a Coherent Pulsed-Doppler Lidar

where  $F_d$  is the Doppler frequency shift,  $V_r$  is the radial velocity of a target, and  $\lambda$  is the wavelength of the signal transmitted. Part of the CW master oscillator beam is split-off, frequency translated, and optically summed with the received target echo signal, and the optically mixed signal is focused onto the photodetector (4).

The photodetector performs as a square-law device with negligible second order terms converting optical energy to electrical energy and creating sum and difference frequency terms (4). The frequency bandwidth of the detector limits the output to only the frequency difference terms; therefore, the output of the photodetector is an electrical signal with a radio frequency (RF) spectrum and a mean frequency equal to the difference between the received signal frequency and the frequency translated master oscillator frequency. This detection procedure is commonly known as optical heterodyne detection.

A well designed coherent optical receiver is a shot noise or quantum noise limited receiver in which the primary source of noise is the shot noise generated by the master oscillator. The additive shot noise of the photodetector is modeled statistically as additive white Gaussian noise over the narrow bandwidth of the detector. With a monochromatic CW oscillator of sufficient power so that other noise sources such as dark current noise and optical background radiation become negligible, the optical receiver can achieve an average signal to noise ratio expressed as:

$$SNR = \frac{\eta P_r}{h\nu B} \quad (2)$$

where

$SNR$  = average signal to noise ratio

$\eta$  = photodetector quantum efficiency

$P_r$  = average power of the received signal with the same polarization as the master oscillator signal (W)

- $h$  = Planck's constant (J·s)  
 $\nu$  = optical frequency incident on photodetector (Hz)  
 $B$  = photodetector bandwidth (Hz)

According to Bachman (1:11-16) when the target echo signal is a coherent, normally incident plane wave, the output of the photodetector is an ensemble average electrical current expressed as:

$$i(t) = \frac{\eta q}{h\nu} \{P_{mo} + P_r(t) + 2[P_{mo}P_r]^{1/2} \cos[2\pi(f_{mo} - f_r)t + \phi_r(t)]\} \quad (3)$$

where

- $\eta$  = photodetector quantum efficiency  
 $q$  = electronic charge (C)  
 $P_{mo}$  = power of the master oscillator CW signal (W)  
 $P_r(t)$  = power of the received signal with the same  
                     polarization as the master oscillator signal (W)  
 $f_{mo}$  = frequency of master oscillator signal plus offset (Hz)  
 $f_r$  = frequency of received signal (Hz)  
 $\phi_r(t)$  = phase difference between the received signal  
                     and the master oscillator signal (rads)

The second term of Equation (3) is the frequency modulated signal of interest.

After heterodyning, the electrical signal is input to the signal processor and computer where either time domain or frequency domain techniques originally developed for millimeter-wave radar are employed. Using classical time domain and frequency domain signal processing techniques, target information such as range and range-rate is obtained. After accounting for atmospheric effects and the receiver SNR from Equation (2) which are different from millimeter-wave radar receivers, Bach-

man concludes that the statistical problem of accurately measuring target range and target radial velocity with a coherent lidar is essentially the same as the detection problem using conventional millimeter-wave radar.

### 2.3 Lidar Theory

Conventional millimeter-wavelength and laser-wavelength pulse-Doppler radars measure the phase difference between subsequently transmitted and reflected pulses to determine hard-target range and radial velocity; whereas, with a diffuse target such as the atmosphere, Doppler lidar measures the Doppler shift of each received pulsed defined by the range-gate of the system. A hard-target is simply defined as a target which is smooth on the scale of the laser wavelength transmitted and reflects the transmitted signal without amplitude or frequency distortion. A diffuse target is rough on the scale of the transmitted laser wavelength which results in multiple reflections of the transmitted signal. Several authors have provided the radar range equation which describes the hard-target detection scenario (37, 1, 20) For the hard-target case where the target is larger than the radar beamwidth and normal to the plane of the optical beam, the radar range equation can be expressed as:

$$P_r(t) = P_t(t - 2R/c) \rho \frac{A_e}{R^2} \eta_{se} \exp \left[ -2 \int_0^R \alpha(R') dR' \right] \quad (4)$$

where

- $P_r(t)$  = expected value of the received power with the  
same polarization as the master oscillator (W)
- $P_t(t)$  = range-delayed power profile of the transmitted signal (W)
- $R$  = range to the target (m)
- $c$  = speed of light (m/s)
- $\rho$  = target reflected power per steradian (sr) divided by the  
incident power (1/sr)

$A_e$  = effective area of the antennae aperture ( $\text{m}^2$ )

$\eta_{se}$  = optical system efficiency

$\alpha(R)$  = two-way extinction coefficient ( $1/\text{m}$ )

In Equation (4) above, some simplifications have been made. The received signal power  $P_r(t)$  represents an average power, and its actual value is slightly less when the atmospheric effects of speckle pattern fluctuation and refractive turbulence are included. For hard-target detection with sufficient SNR, turbulence effects and the aerosol volume backscatter coefficient  $\beta(R)$  ( $1/\text{m} \times 1/\text{sr}$ ) become negligible. The power profile of the return signal range delayed in time is the same as the transmitted power profile; however, for the case of a diffuse target such as a volume of aerosols, the returned signal power profile changes significantly.

For the diffuse target case, the radar range equation (20:2) can be expressed as:

$$P_r(t) = \int_{c(t-\tau)/2}^{ct/2} P_t(t - 2R/c) \beta(R) \frac{A_e}{R^2} \eta_{sr} \exp \left[ -2 \int_0^R \alpha(R') dR' \right] dR \quad (5)$$

where  $\tau$  is the pulse duration. Again, the effect of turbulence has been ignored. If strong turbulence is present, an additional turbulence factor to reduce  $P_r$  is required. The ensemble average power profile  $P_r(t)$  depends on the cumulative effect of the backscattered radiation from a large number of aerosols within the illuminated volume which is defined by the beam width and the pulse duration. The integration over  $R$  of Equation (5) indicates that at time  $t$ , the aerosols within a slab of atmosphere of thickness  $c\tau/2$  and centered at  $R = c(t/2 - \tau/4)$  backscatter radiation to form the power profile  $P_r(t)$  (20). Therefore, the range resolution defined by  $c\tau/2$  is relatively coarse compared to a conventional pulse detection Doppler radar. For a typical  $\text{CO}_2$  transmitter with a pulse duration of  $1 \mu\text{s}$ , the range resolution is approximately 150 m. If the pulse duration is reduced to improve range resolution,

the resultant spread of the frequency spectrum of the transmitted signal will result in a significant loss of frequency (velocity) resolution.

Therefore, the classical trade-off between range and velocity resolution as determined by the pulse duration of the transmitted signal exists for lidar diffuse target applications as well as conventional Doppler radar hard-target applications. According to Menzies and Hardesty, the accuracy of Doppler lidar velocity measurements depend on two fundamental parameters: the SNR and the spectral width of the backscattered signal (24).

#### *2.4 Lidar Signal Processing*

Although this thesis does not directly apply lidar signal processing techniques, a brief introduction to current lidar wind sensing signal processing techniques is given to provide a complete overview of lidar theory. Current lidar wind sensing systems typically employ three stages of signal processing: amplification and complex demodulation, analog to digital (A/D) conversion, and either frequency domain or time domain digital signal analysis. After the received signal from the photodetector is amplified, filtered, converted to quadrature components, and digitized, the signal parameters of interest are estimated using one of the two signal processing techniques developed. These two techniques are Fourier spectral analysis and covariance analysis. Fourier spectral analysis is a relatively straight forward method of obtaining an estimate of the power spectral density (PSD) of the received signal which is referred to as a periodogram. Three parameters of the periodogram of primary interest are the following: the mean power, the mean frequency, and the frequency width. In comparison to Fourier spectral analysis, the covariance technique is a less computationally intense method of obtaining estimates of these three parameters. In this section, complex demodulation, A/D conversion, and PSD parameter estimation for current lidar systems are briefly reviewed.

Complex demodulation structures such as the one illustrated in Figure 2 typically consist of a bandpass filter broad enough to receive the Doppler-shifted signal  $s_{r1}(t)$  from the photodetector output. The signal  $s_{r1}(t)$  is filtered and amplified to produce the intermediate signal  $s_{r2}(t)$ . The signal  $s_{r2}(t)$  is divided into two channels called the I and Q channels for in-phase and quadrature respectively. Mixing  $s_{r2}(t)$  with the single frequency terms  $\sin(2\pi f_o t)$  and  $\cos(2\pi f_o t)$  and low pass filtering forms the in-phase and quadrature components of  $s_{r2}(t)$ . The low pass filter (LPF) of each channel preserves the frequency difference signals and eliminates the frequency sum signals associated with the mixing process. The mixing and filtering of  $s_{r2}(t)$  to obtain the I and Q components of  $s_{r2}(t)$  provides a means of determining the direction of the radial velocity relative to the lidar. After sampling the I and Q channels, the digital output signal can be written as

$$s_{r3}(nT_s) = i(nT_s) + q(nT_s) \quad (6)$$

where  $T_s$  is the sampling period and  $n = 0, 1, \dots, N - 1$ . The digitized output signal  $s_{r3}(nT_s)$  is sent to a computer with the software routines necessary for either spectral or covariance processing to estimate the signal parameters of interest.

First consider the case of Fourier spectral processing. Discrete Fourier transform (DFT) methods are employed to obtain the periodogram for each range bin of  $s_{r3}(nT_s)$ . The width of the range bin for each periodogram derived is determined by the number of digital samples  $N$  of the DFT. Coherent Technologies Incorporated (CTI) has developed a Fourier spectral processor for lidar wind sensing. The spectral signal processing of the CTI lidar (42:41-42) can be summarized in the following steps:

Step 1. Obtain the DFT (nominal length  $N = 128$  samples) of  $s_{r3}(nT_s)$  expressed as:

$$Z(kf_{res}) = \sum_{n=0}^{N-1} s_{r3}(nT_s) \exp(-j2\pi nT_s kf_{res}) \quad (7)$$

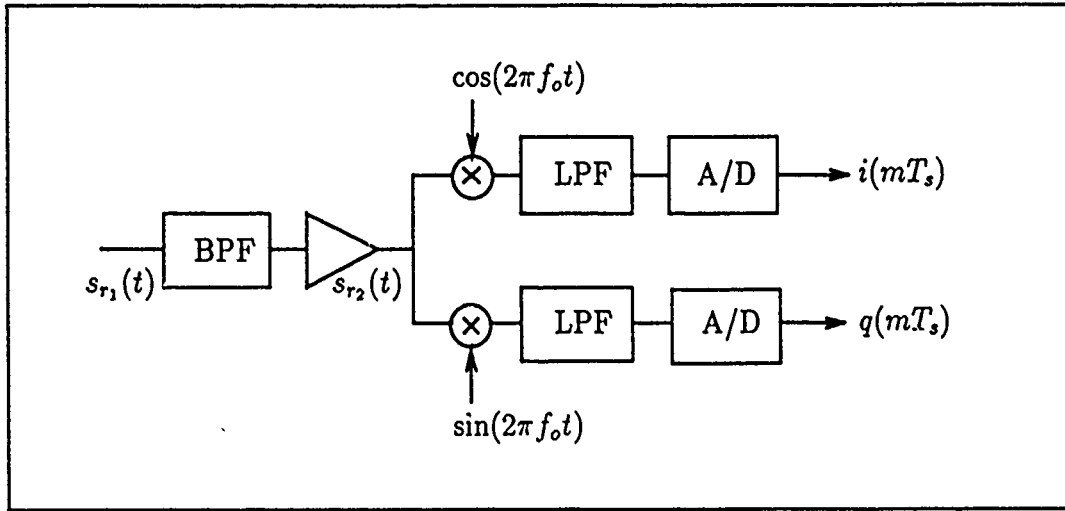


Figure 2. Complex Demodulator

where  $f_{\text{res}} = 1/NT_s$  and  $k = 0, 1, \dots, N - 1$ .

Step 2. For each range bin, determine the periodogram expressed as

$$S(kf_{\text{res}}) = \frac{T_s}{N} |Z(kf_{\text{res}})|^2 \quad (8)$$

Step 3. Store the periodogram for each range bin in memory, transmit additional pulses (perhaps as many as 1000) and repeat the process storing all periodogram data in memory.

Step 4. After transmitting, processing, and storing the data during the time interval in which the random process describing the backscattered signal is assumed stationary (refer to Chapter 3 for details), the periodogram data can be edited and averaged to eliminate spurious signals. The edited and averaged periodogram for each range bin designated as  $\bar{S}(kf_{\text{res}})$  for a large number of averaged pulses is expected to yield a symmetric Gaussian spectrum. Therefore, the central moments of  $\bar{S}(kf_{\text{res}})$  yield the desired signal parameters of mean power, mean Doppler frequency, and Doppler variance.



Step 5. Compute the first three central moments of  $\bar{S}(kf_{\text{res}})$ . The zero moment estimate is expressed as

$$\hat{P}(R) = \sum_{k=0}^{N-1} \bar{S}(kf_{\text{res}}) \quad (9)$$

where  $\hat{P}(R)$  represents the estimated average power backscattered from range bin  $R$ . The range bin  $R$  is defined as  $R = (c/2)(N \times T_s)$ . The estimate of the first moment of  $\bar{S}(kf_{\text{res}})$  converted to radial velocity coordinates is expressed as

$$\bar{V}_r(R) = \frac{-\lambda}{2N} \left\{ \frac{k_m}{T_s} + \frac{1}{\hat{P}(R)T_s} \sum_{k_m - \frac{N}{2}}^{k_m + \frac{N}{2}} (k - k_m) \bar{S}[\text{mod}_N(k)] \right\} \quad (10)$$

where  $\lambda$  is the wavelength transmitted and  $k_m = k_{\text{max}}$ , the spectral coefficient of the greatest magnitude.  $\bar{V}_r(R)$  is the estimated average radial velocity at a given range bin. The estimate of the second central moment or the variance of  $\bar{S}(kf_{\text{res}})$  for each range bin is expressed as

$$\hat{\sigma}_V^2(R) = \frac{\lambda^2}{4\hat{P}(R)T_s^2} \sum_{k_m - \frac{N}{2}}^{k_m + \frac{N}{2}} \left( \frac{k}{N} + \frac{2\bar{V}_r(R)T_s}{\lambda} \right)^2 \bar{S}[\text{mod}_N(k)] \quad (11)$$

The estimate of the velocity width is given as

$$\hat{\sigma}_V(R) = [\hat{\sigma}_V^2(R)]^{1/2} \quad (12)$$

The first three moment estimates of  $\bar{S}(kf_{\text{res}})$  designated as  $\hat{P}(R)$ ,  $\bar{V}_r(R)$ , and  $\hat{\sigma}_V(R)$  provide the information of interest. The first three moments provide the mean power estimate which indicates the aerosol density, the mean aerosol radial velocity estimate which indicates the mean radial wind velocity, and the spectral width estimate which indicates the degree of relative wind velocity due to atmospheric turbulence.

Next consider the covariance processing technique. This technique is analogous to the pulse-pair signal processor implemented in conventional microwave, Doppler meteorological radar. Using the single-lag autocovariance processor (SLA) (11:91-

119) one obtains the first three estimated moments of the received signal PSD. The instantaneous power backscattered can be expressed in terms of the squared components of  $s_{r_3}(nT_s)$  due to pulse  $m$  as

$$P_m(nT_s) = I^2(nT_s) + Q^2(nT_s) \quad (13)$$

Averaging the instantaneous samples of  $P_m(nT_s)$  determines the mean backscattered signal power expressed as

$$\hat{P}(R) = \frac{1}{N} \frac{1}{M} \sum_{m=0}^{M-1} \sum_{n=0}^{N-1} P_m(nT_s) \quad (14)$$

where

$\hat{P}(R)$  = the estimate of average power at range bin  $R$  (W)

$R$  = the range bin width where  $R = (c/2)(N \times T_s)$

$N$  = number of digital samples within a range bin

$M$  = number of pulses averaged

The average signal power estimate less the white Gaussian noise term  $N$  of the photodetector can be expressed as

$$\hat{S}(R) = \hat{P}(R) - N \quad (15)$$

From Doviak and Zrnic (11:91-119), the SLA processor forms an estimate of the complex autocorrelation function expressed as

$$\hat{R}(T_s) = \frac{1}{N} \sum_{n=1}^{N-1} s_{r_3}(nT_s) s_{r_3}[(n+1)T_s] \quad (16)$$

For symmetric spectra, the unbiased mean radial velocity estimate can be expressed in terms of the argument of the complex autocorrelation function estimate  $\hat{R}(T_s)$  as

$$\bar{V}_r(R) = \frac{-\lambda}{4\pi T_s} \arg \{ \hat{R}(T_s) \} \quad (17)$$

The spectral width  $\hat{\sigma}_V$  of an assumed symmetric Gaussian spectrum can be expressed in terms of  $\hat{R}(T_s)$  and  $\hat{S}(R)$  of Equations (15) and (16) as

$$\hat{\sigma}_V = \frac{\lambda}{2^{3/2}\pi T_s} \left| \ln \left( \frac{\hat{S}}{|\hat{R}(T_s)|} \right) \right|^{1/2} \text{sgn} \left[ \ln \left( \frac{\hat{S}}{|\hat{R}(T_s)|} \right) \right] \quad (18)$$

where the sgn term identifies possible negative terms due to low signal-to-noise ratio. For more details of the derivations to obtain Equations (17) and (18), refer to the text of Doviak and Zrnic (11:91-11).

There are advantages and disadvantages associated with each signal processing technique. For more detailed discussions of the variances associated with the spectral and covariance estimators and comparisons of each in terms of their advantages and disadvantages, refer to the references provided (11, 42, 36).

When implementing either processing technique, the lidar range resolution is a function of the range bin length  $R$  with  $N$  samples, the pulse duration  $T$ , and the bandwidth  $B$  of the receiver electronics. For example, the CTI lidar (42:41) operates with the following nominal aerosol measurement parameters:  $T = 1\mu s$ ,  $T_s = 10ns$ , and  $N = 128$  samples centered at each range bin. With the CTI system, computing the first three moments of the periodogram (as in Steps 1-5) provides a range resolved profile of the wind the lidar pulse encounters as it propagates through the atmosphere. The range bin consisting of 128 samples spaced 1.5 m apart in range forms a range bin with of  $R = (c/2)(N \times T_s) = 192m$ . The samples taken at each range bin must occur within the coherence time of the received signal; otherwise, random modulation of the received signal broadens the frequency spectrum. This

aspect of the backscattered signal is discussed in more detail in Chapter 3.

Sampling in range to form the range bin reduces the range resolution of the system because the time duration required to form the  $N$  sample range bin  $R$  results in samples from a pulse which has propagated in range. In other words, during the time required to obtain the 128 samples within a range bin, the pulse effectively smears through additional aerosol scatterers to form a larger scattering volume. The scattering volume is defined in terms of the lidar beamwidth and the spatial extent of the transmitted pulse expressed as  $cT/2$ . In addition, the bandwidth of the lidar will determine the degree of spatial averaging of the scattering volume. In other words, a finite bandwidth receiver averages the backscattered signal. Therefore, due to pulse width and bandwidth constraints of the lidar system, range resolution is typically greater than the range bin width  $R$  defined by the DFT length  $N$ . Range resolution is discussed in greater detail in Chapters 3 and 4.

This section has provided a basic overview of existing lidar signal processing techniques for the dense aerosol target environment. It can be shown that Fourier spectral processing is comparable to approximate matched-filter radar receivers when the spectral coefficients of the DFT are equally weighted and the DFT length is comparable to the time duration of the transmitted rectangular pulse (14:82-84). In the next chapter, the theory of matched-filter radar as it applies to a dense aerosol target environment is developed, and matched-filter signal processing is compared to the Fourier spectral processing technique.

### *III. Theory and Methods*

#### *3.1 Introduction*

The primary purpose of this thesis effort is to consider alternative conventional radar signals to the simple unmodulated pulse currently in use with existing lidars to determine whether these alternative signals offer some means of improving the resolution of aerosol measurements. To accomplish this purpose, two general models are required: a model of the general lidar receiver and a model to describe the aerosol target. Section 3.2 discusses the basic theory of matched-filter (MF) radar receiver design. Section 3.3 describes resolution properties of the receiver in terms of the radar ambiguity function. Section 3.4 characterizes the complex target which consists of a dense array of point targets distributed in range and frequency. And finally, Section 3.5 combines these two models to describe the general matched-filter square-law receiver (MFSLR) response to the complex target. The developments presented in Sections 3.2 through 3.5 provide the essential tools necessary for determining range and velocity resolution of various radar signals with respect to the aerosol, dense target model.

#### *3.2 Matched-Filter Theory*

Development of the matched-filter receiver for the aerosol sensing lidar was chosen because it was seen to provide the simplest and most commonly employed method of evaluating various signals to determine their measurement capability with respect to a myriad of possible target scenarios. Throughout the history of radar development, the ambiguity function based on the matched-filter response has been a fundamental measurement tool to describe radar performance in terms of resolution, accuracy, and ambiguity. The matched-filter receiver is designed to provide optimal signal detection and parameter estimation of an idealized point target of unknown range and radial velocity in white Gaussian noise as illustrated in numerous texts

(38, 26). According to Van Trees (39:276-279) the matched-filter receiver followed by a square-law envelope detector will provide the maximum-likelihood estimates of point target range and radial velocity when the receiver noise is Gaussian. Whether the matched-filter receiver followed by a square-law envelope detector is the optimal receiver in a dense target environment such as aerosols is less clear as Rihaczek and Van Trees indicate (39, 30). However, a basic assumption of this thesis effort is to determine resolution performance in terms of a conventional matched-filter radar receiver design.

Consider the simplified radar model where the target is assumed to be a single point target. If the target is in motion, the received signal is represented as a time-delayed, Doppler-shifted version of the transmitted signal corrupted by white Gaussian noise from the shot-noise limited photodetector. For this model, it is assumed that the point target radial velocity remains constant over the pulse duration. In other words, higher order target acceleration terms are negligible. (30:56-65) Thus the transmitted pulse is expressed as

$$s(t) = m(t) \exp(j2\pi f_c t) \quad (19)$$

where

$s(t)$  = transmitted signal expressed in complex form (V)

$m(t)$  = complex modulation function (V)

$f_c$  = carrier frequency (Hz)

The use of complex signal notation is assumed throughout the thesis, so a signal is assumed to be complex unless stated otherwise. The magnitude of  $m(t)$  is the envelope of the real signal. The transmitted signal represented in complex baseband form is simply expressed as

$$s(t) = m(t) \quad (20)$$

Ignoring changes of amplitude, the signal backscattered from the point target can be represented as

$$s_r(t) = m(t - \tau_d) \exp[j2\pi(f_c + f_d)(t - \tau_d)] + n(t) \quad (21)$$

where

$$\tau_d = cR/2$$

$$f_d = -2V_r/\lambda$$

and where

$\tau_d$  = range-delay time due to the point target range  $R$  (s)

$f_d$  = Doppler frequency-shift due to the point  
target radial velocity (Hz)

$c$  = speed of light (m/s)

$\lambda$  = transmitted signal wavelength (m)

$n(t)$  = white Gaussian noise signal (V)

Conversion of the received signal to complex baseband form yields

$$s_r(t) = m(t - \tau_d) \exp(j2\pi f_d t + j\phi) + n(t) \quad (22)$$

where  $\phi = 2\pi(f_c + f_d)\tau_d$  radians. The task of the receiver is the accurate estimation of the parameters  $\tau_d$  and  $f_d$  assuming neither parameter is known apriori. This is the classical radar problem and references discussing its many applications abound (38, 30, 39, 26). Radar texts commonly demonstrate the optimality of matched-filter detection of the backscattered signal from a single point target in white Gaussian noise (38:369-376). If the target is stationary, a single, linear time-invariant matched-filter (MF) is adequate to achieve maximum likelihood estimation of target range-time delay  $\tau_d$ . The MF impulse response  $h(t)$  which maximizes the peak signal to

mean noise power ratio, can be expressed in terms of the transmitted signal as

$$h(t) = s^*(-t) \quad (23)$$

The matched-filter frequency transfer function  $H(f)$  is expressed through the Fourier transform of Equation (23) as

$$H(f) = S^*(f) \quad (24)$$

First consider the stationary point target case where  $f_d = 0$ , and the only target parameter to estimate is the range time-delay  $\tau_d$ . For this case, Equation (22) simplifies to

$$s_r(t) = m(t - \tau_d) \exp(j\phi) + n(t) \quad (25)$$

where  $\phi = 2\pi f_c \tau_d$ . One can easily show that the MF response  $y(\tau)$  can be expressed as

$$y(\tau) = \int_{-\infty}^{\infty} s_r(t) s^*(t - \tau) dt \quad (26)$$

The form of Equation (26) shows that the matched filter response is obtained through a cross-correlation of the received signal with a time shifted replica of the transmitted signal. Substituting Equation (25) into Equation (26) and neglecting the noise term  $n(t)$  yields

$$y(\tau) = \exp(j\phi) \int_{-\infty}^{\infty} s(t - \tau_d) s^*(t - \tau) dt = \exp(j\phi) R(\tau - \tau_d) \quad (27)$$

where  $R(\tau - \tau_d)$  represents the time-shifted autocorrelation function of the transmitted signal. The MF response can also be expressed in terms of the complex modulation envelopes as

$$y(\tau) = \exp(j\phi) \int_{-\infty}^{\infty} m(t - \tau_d) m^*(t - \tau) dt = \exp(j\phi) R(\tau - \tau_d) \quad (28)$$

Where in this case  $R(\tau - \tau_d)$  represents the time-shifted autocorrelation function of



the complex modulation envelope of the transmitted signal. Since the phase  $\phi$  is unknown, envelope detection is required. If a square-law envelope detector follows the MF, the matched-filter square-law receiver (MFSLR) output can be expressed as

$$|y(\tau)|^2 = |R(\tau - \tau_d)|^2 \quad (29)$$

where the peak of  $|R(\tau - \tau_d)|^2$  occurs at  $\tau = \tau_d$ . This type of estimation is referred to as noncoherent estimation since the target phase information is eliminated.

Now consider the non-stationary point target case in which the point target parameters  $\tau_d$ ,  $f_d$ , and  $\phi$  are unknown. For this case, the received signal, neglecting the Gaussian noise term can be expressed as

$$s_r(t) = s(t - \tau_d) \exp(j2\pi f_d t + j\phi) \quad (30)$$

Since both  $\tau_d$  and  $f_d$  are unknown, an array of matched-filters with incrementally spaced center-frequencies as illustrated in Figure 3 is required to extract the maximum-likelihood estimates of  $\tau_d$  and  $f_d$ . If the filters of the MF array of Figure 3 are spaced with infinitesimally small center-frequency increments, the array MF response can be expressed as

$$y(\tau, f) = \int_{-\infty}^{\infty} s_r(t) s^*(t - \tau) \exp(-j2\pi f t) dt \quad (31)$$

The form of Equation (31) shows that the MF response consists of the cross-correlation of the received signal with a time-shifted, frequency-shifted version of the transmitted signal (30:69). The received signal of Equation (30) substituted into Equation (31) yields

$$y(\tau, f) = \exp(j\phi) \int_{-\infty}^{\infty} s(t - \tau_d) s^*(t - \tau) \exp[-j2\pi(f - f_d)t] dt \quad (32)$$

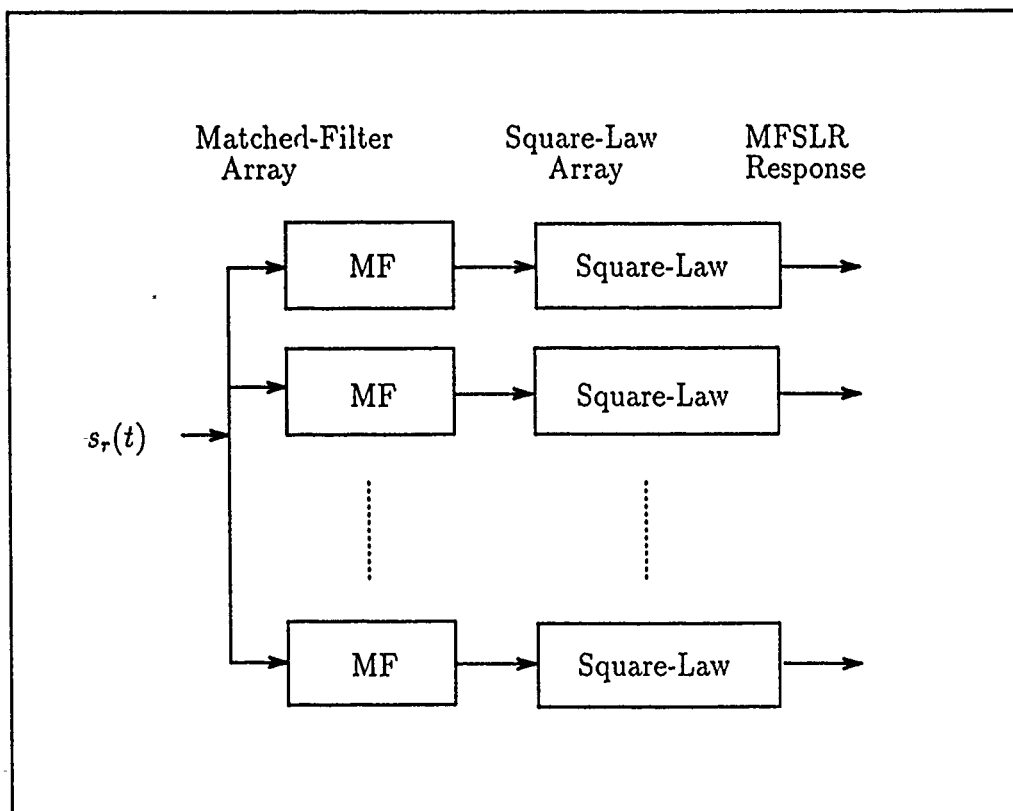


Figure 3. Matched-Filter, Square-Law Receiver

Since envelope detection is typically employed, the phase term is neglected, and the MF response can be expressed as

$$y(\tau, f) = \int_{-\infty}^{\infty} s(t) s^*[t - (\tau - \tau_d)] \exp[-j2\pi(f - f_d)] dt \quad (33)$$

With the change of variables

$$\tau' = \tau - \tau_d \quad (34)$$

$$f' = f - f_d \quad (35)$$

the MF response of Equation (33) simplifies to

$$y(\tau', f') = \int_{-\infty}^{\infty} s(t) s^*(t - \tau') \exp(-j2\pi(f') dt \quad (36)$$

The variable translations of Equations (34) and (35) shift the MF response from the target location  $(\tau_d, f_d)$  in the  $(\tau, f)$  plane to the origin of the  $(\tau', f')$  plane.

Equation (36) represents the MF response neglecting the unknown phase term and the noise term of Equation (25). This function, first introduced to radar theory by Woodward (41:118-119), is called the signal ambiguity function. For a complex transmitted signal  $s(t)$ , the ambiguity function is defined as

$$\chi(\tau, f) = \int_{-\infty}^{\infty} s(t) s^*(t - \tau) \exp(-j2\pi ft) dt \quad (37)$$

where the prime notation has been dropped. The ambiguity function represents the MF response with its axes centered at the target location  $(\tau_d, f_d)$ . In terms of the complex low pass envelope of  $s(t)$ , the ambiguity function is expressed as

$$\chi(\tau, f) = \int_{-\infty}^{\infty} m(t) m^*(t - \tau) \exp(-j2\pi ft) dt \quad (38)$$

The ambiguity function can also be expressed in its symmetrical form as

$$\chi(\tau, f) = \int_{-\infty}^{\infty} m(t + \tau/2)m^*(t - \tau/2)\exp(-j2\pi ft)dt \quad (39)$$

The MFSLR response (as in Figure 3) is the squared-modulus of  $\chi(\tau, f)$  and is designated with the symbol  $\theta(\tau, f)$  where

$$\theta(\tau, f) = \left| \int_{-\infty}^{\infty} m(t + \tau/2)m^*(t - \tau/2)\exp(-j2\pi ft)dt \right|^2 \quad (40)$$

$\theta(\tau, f)$  is also commonly referred to as the ambiguity function, and the three dimensional plot of the surface of  $\theta(\tau, f)$  above the  $(\tau, f)$  plane is called the ambiguity diagram.

Several mathematical properties of the ambiguity function  $\theta(\tau, f)$  can be found in numerous radar texts (39, 38). These properties are typically given in terms of a transmitted signal  $s(t)$  which is normalized with respect to its energy such that

$$\int_{-\infty}^{\infty} |s(t)|^2 dt = 1 \quad (41)$$

If the transmitted signal is normalized such that Equation (41) is satisfied, some useful properties of the ambiguity function (39, 38) can be stated in the following equations:

$$\text{Ambiguity Volume} = \int \int_{-\infty}^{\infty} \theta(\tau, f) d\tau df = 1 \quad (42)$$

$$\text{Max}\{\theta(\tau, f)\} = \theta(0, 0) = 1 \quad (43)$$

$$\theta(\tau, 0) = \left| \int_{-\infty}^{\infty} m(t)m^*(t - \tau)dt \right|^2 \quad (44)$$

$$\theta(0, f) = \left| \int_{-\infty}^{\infty} m^2(t)\exp(-j2\pi ft)dt \right|^2 \quad (45)$$

$$\theta(\tau, f) = \theta(-\tau, -f) \quad (46)$$

Equation (42) is known as the volume invariance property which indicates that the

volume of a normalized ambiguity function always equals unity. Equation (43) indicates that the maximum of the normalized ambiguity function always occurs at the origin and equals unity. Equations (44) and (45) indicate the form of the ambiguity function across the range-time delay and frequency axes respectively. Equation (46) is a symmetry relationship. The volume invariance property and the maximum amplitude property describe the fundamental limitation of radar resolution performance.

Another useful function in radar theory is the cross ambiguity function (26:286) defined as

$$\chi_c(\tau, f) = \int_{-\infty}^{\infty} s_1(t) s_2^*(t - \tau) \exp(-j2\pi ft) dt \quad (47)$$

Substituting  $s_r(t)$  as expressed in Equation (25) for  $s_1(t)$  and substituting the transmitted signal for  $s_2(t)$ , the cross ambiguity function represents the MF response given as

$$\chi_c(\tau, f) = \exp(j\phi) \chi(\tau, f) + \chi_n(\tau, f) \quad (48)$$

where

$$\chi_n(\tau, f) = \int_{-\infty}^{\infty} n(t) s^*(t - \tau) \exp(-j2\pi ft) dt \quad (49)$$

Equation (48) represents the MF response in terms of the signal component and Gaussian noise component of the received signal. The cross ambiguity function represents a statistic for estimating  $\tau_d$  and  $f_d$ . If  $f_d$  is known, the peak of  $|\chi_c(\tau, f_d)|^2$  along the  $\tau$  axis determines  $\tau_d$ . If  $\tau_d$  is known, the peak of  $|\chi_c(\tau_d, f)|^2$  along the  $f$  axis determines  $f_d$ . If neither  $\tau_d$  nor  $f_d$  are known, the peak of  $|\chi_c(\tau, f)|^2$  in the  $(\tau, f)$  plane determines  $\tau_d$  and  $f_d$  with maximum likelihood (8:8-58-8-59).

### 3.3 Radar Resolution

Radar resolution is defined in terms of the radar's capability to separate signals due to point targets which are separated in range or in radial velocity or in both range and radial velocity. Radar resolution is analyzed based on the premise that the signal

can be detected in the receiver noise; otherwise, analysis of resolution capability is irrelevant. In general, the signal ambiguity function without considering noise effects is required for determining radar resolution performance (30:1-9). Recall from Equations (34) and (35) of Section 3.2 that the definition of the ambiguity function  $\chi(\tau, f)$  is in terms of the MF response translated to the target coordinates  $(\tau_d, f_d)$ . Substitution of Equations (34) and (35) into Equation (38) yields the expression for the MF response in the  $(\tau, f)$  plane which can be expressed as

$$y(\tau, f) = \exp(j\phi)\chi(\tau - \tau_d, f - f_d) \quad (50)$$

Next, consider the case where numerous point targets are imaged. In a dense target environment, the radar beam illuminates many closely-spaced point targets. If  $\sigma(\tau_{d_n}, f_{d_n})$  represents the backscattering cross section of the  $n$ th point target and  $\phi(\tau_{d_n}, f_{d_n})$  represents the phase of the  $n$ th point target, the MF response, neglecting the Gaussian noise term, becomes a superposition of the MF responses from the backscattered signals from each point target. The resultant MF output can be expressed as

$$y(\tau, f) = \sum_{n=1}^N \sigma^{1/2}(\tau_{d_n}, f_{d_n}) \exp[j\phi(\tau_{d_n}, f_{d_n})] \chi(\tau - \tau_{d_n}, f - f_{d_n}) \quad (51)$$

where

$N$  = number of particles illuminated

$\sigma^{1/2}(\tau_{d_n}, f_{d_n})$  = reflectivity of the  $n$ th point target

$\phi(\tau_{d_n}, f_{d_n})$  = unknown phase of the  $n$ th point target (rads)

In the limit as the number of particles becomes infinite, the target becomes continuous in range and radial velocity, and the MF response is given as

$$y(\tau, f) = \int \int_{-\infty}^{\infty} \sigma^{1/2}(\tau_d, f_d) \exp[j\phi(\tau_d, f_d)] \chi(\tau - \tau_d, f - f_d) d\tau_d df_d \quad (52)$$

The form of Equations (51) and (52) shows that the MF response is expressed in terms of a coherent superposition of the amplitudes and phases of each point target. As a result, the MF response as expressed in Equations (51) and (52) is called coherent imaging (8:7-12-7-13). As Rihaczek explains, in a dense target environment where the radar illuminates numerous point targets, the differential ranges between point targets are essentially random. Therefore attempts to determine the exact coherent superposition of amplitudes and phases to describe the MF response is unrealistic (30:111-114).

To proceed with the discussion of resolution, a statistical approach is required. Rihaczek shows that the dense target environment requires a statistical description of the target backscatter and its corresponding MF response in terms of the mean target backscatter cross section  $\bar{\sigma}$  and the mean power response of the MF  $\overline{y^2}$ . The mean power response can be obtained with the MFSLR illustrated in Figure 3. If  $\bar{\sigma}(\bar{\tau}_{d_n}, \bar{f}_{d_n})$  represents the average cross section of the nth target where  $\bar{\tau}_{d_n}$  and  $\bar{f}_{d_n}$  represent the mean range time-delay and Doppler frequency-shift of the nth target, Rihaczek shows that the MFSLR response can be expressed as

$$\overline{|y(\tau, f)|^2} \simeq \sum_{n=1}^N \bar{\sigma}(\bar{\tau}_{d_n}, \bar{f}_{d_n}) \theta(\tau - \bar{\tau}_{d_n}, f - \bar{f}_{d_n}) \quad (53)$$

Again, in the limit as the point targets become continuous in range and frequency, Rihaczek expresses the average MFSLR response as

$$\overline{|y(\tau, f)|^2} \simeq \int \int_{-\infty}^{\infty} \bar{\sigma}(\bar{\tau}_d, \bar{f}_d) \theta(\tau - \bar{\tau}_d, f - \bar{f}_d) d\bar{\tau}_d d\bar{f}_d \quad (54)$$

Equation (54) describes a two-dimensional convolution of the average scattering function with the waveform ambiguity function. Unfortunately, limitations exist concerning the validity of Equations (53) and (54) in terms of imaging aerosols. In the Rihaczek derivation of these equations, he states the assumption that the target consists of a fixed distribution of scatterers in range and radial velocity. In

other words, the orientation of the particles with respect to the radar does not change significantly over the time duration of the transmitted pulse. (30:335-338) This limitation is especially bothersome when imaging aerosols which rapidly change their orientation. If the pulse duration of the transmitted signal is short enough (i.e. within the coherence time  $\approx 1 - 10\mu\text{s}$ ) such that significant changes of the aerosol orientations with respect to each other do not occur during the measurement interval, Equations (53) and (54) are valid approximations of the mean MFSLR response. Later in Sections 3.4 and 3.5 a similar but more general result for the mean power MFSLR response is obtained. For now, assuming Equations (53) and (54) are valid, they can be used to illustrate some useful concepts of resolution.

The form of Equation (54) shows that the average MFSLR response is obtained through a superposition of  $\theta(\tau, f)$  for each point target. Also, Equation (54) provides a simple analytical description of the mean MFSLR response in a dense target environment. One can think of the average scattering function  $\bar{\sigma}(\bar{\tau}_d, \bar{f}_d)$  as a two-dimensional input, the ambiguity function  $\theta(\tau, f)$  as an impulse response of a two-dimensional linear filter, and the mean MFSLR response  $\bar{y}^2$  as the two-dimensional output of the filter. If the ambiguity function could be represented as the two-dimensional impulse function  $\delta(\tau, f)$  its substitution into Equation (54) would yield

$$\overline{|y(\tau, f)|^2} = \bar{\sigma}(\tau, f) \quad (55)$$

The two-dimensional delta ambiguity function represents a radar with infinitesimal resolution in time and frequency or alternatively in range and radial velocity. Based on this idealized response, a radar meteorologist can infer common parameters of interest pertaining to the target such as backscatter density, mean velocity, and velocity spread. These parameters are obtained from the complete knowledge of  $\bar{\sigma}(\tau, f)$ . It is well known that the delta ambiguity function is unrealizable in both the  $\tau$  and  $f$  axes simultaneously. A realizable radar ambiguity function will have finite widths  $\Delta\tau$  and  $\Delta f$  in range time-delay (RTD) and Doppler frequency-shift



(DFS). It is clear that target resolution is only as good as the filter resolution with which it is observed; therefore, the shape of the ambiguity function  $\theta(\tau, f)$  and its distribution over the  $(\tau, f)$  axis is fundamental to determining resolution.

Three commonly referenced resolution criteria are the Woodward, the Rayleigh, and the half-power criteria. The Woodward resolution criterion (41:118-119) for RTD resolution width can be expressed as

$$\Delta\tau = \frac{\int_{-\infty}^{\infty} \theta(\tau, 0) d\tau}{\theta(0, 0)} \quad (56)$$

Equation (56) represents the central width  $\Delta\tau$  in which the energy of the ambiguity function is located with respect to the  $\tau$  axis. Assuming the transmitted waveform is normalized with respect to its energy and substituting Equation (42) of Section 3.2 into Equation (56) yields

$$\Delta\tau = \int_{-\infty}^{\infty} \theta(\tau, 0) d\tau \quad (57)$$

Substituting Equation (44) of Section 3.2 into Equation (57) yields

$$\Delta\tau = \int \left| \int_{-\infty}^{\infty} m(t) m^*(t - \tau) dt \right|^2 d\tau \quad (58)$$

If  $M(f)$  represents the Fourier transformation of  $m(t)$ ,  $\Delta\tau$  of Equation (58) can be expressed as

$$\Delta\tau = \int_{-\infty}^{\infty} |M(f)|^4 df \quad (59)$$

As an example, let the normalized complex envelope of the transmitted signal spectrum be expressed as

$$|M(f)| = \frac{1}{B^{1/2}} \text{rect}(f/B) \quad (60)$$

where  $B$  is the bandwidth and where the function  $\text{rect}(f/B)$  is defined as

$$\text{rect}\left(\frac{f}{B}\right) = \begin{cases} 1 & |f| \leq \frac{B}{2} \\ 0 & \text{elsewhere} \end{cases} \quad (61)$$

Substituting Equation (60) into Equation (59) yields

$$\Delta\tau = \int_{-\infty}^{\infty} \left| \frac{1}{B^{1/2}} \text{rect}(f/B) \right|^4 df = 1/B \quad (62)$$

Therefore, the total resolution width in RTD is inversely proportional to the signal bandwidth  $B$ . As the signal bandwidth increases, the RTD resolution improves proportionately. Similarly, the Woodward DFS resolution criterion for a normalized ambiguity function is defined as

$$\Delta f = \int_{-\infty}^{\infty} \theta(0, f) df \quad (63)$$

Substituting Equation (45) from Section 3.2 into Equation (63) and again assuming the signal energy is normalized, DFS resolution can be written as

$$\Delta f = \int_{-\infty}^{\infty} |m(t)|^4 dt \quad (64)$$

And a similar example for DFS resolution width follows where the transmitted signal envelope is expressed as

$$|m(t)| = \frac{1}{T^{1/2}} \text{rect}(t/T) \quad (65)$$

where  $m(t)$  is a normalized rectangular pulse of time-duration  $T$ . The DFS resolution width is obtained from the following equation:

$$\Delta f = \int_{-\infty}^{\infty} \left| \frac{1}{T^{1/2}} \text{rect}(t/T) \right|^4 dt = 1/T \quad (66)$$

full width across the  $\tau$  or  $f$  axis respectively such that  $\theta(\tau, f) = 1/2$ . The RTD resolution width is found by solving for  $\Delta\tau$  in the following equation:

$$\theta\left(\frac{\Delta\tau}{2}, 0\right) = \frac{1}{2} \quad (71)$$

Similarly, the DFS resolution width is found by solving for  $\Delta f$  in the following equation:

$$\theta\left(0, \frac{\Delta f}{2}\right) = \frac{1}{2} \quad (72)$$

For the simple rectangular pulse, the RTD resolution width and the DFS resolution width is usually approximated respectively as

$$\Delta\tau = T \simeq 1/B \quad (73)$$

$$\Delta f = 1/T \simeq B \quad (74)$$

In general, range delay resolution width is inversely proportional to the signal bandwidth and frequency resolution width is inversely proportional to the signal time duration (30:93-98). One can define a nominal resolution cell with dimensions in frequency and range-time delay as

$$\Delta\tau\Delta f = \frac{1}{TB} \quad (75)$$

where  $TB$  is referred to in radar literature as the time-bandwidth product of the transmitted waveform. The RTD resolution expressed in range coordinates is

$$\Delta R = c \times \Delta\tau/2 \quad (76)$$

And the conversion of DFS resolution to radial velocity resolution becomes

$$\Delta V_r = \lambda \times \Delta f/2 \quad (77)$$

Substitution of Equations (76) and (77) into Equation (75) yields the nominal resolution cell with dimensions in range and radial velocity expressed as

$$\Delta R \Delta V_r = \frac{c\lambda}{4} \times \frac{1}{TB} \quad (78)$$

The form of Equation (78) indicates that the area of the nominal resolution cell is directly proportional to the wavelength transmitted and inversely proportional to the signal time-bandwidth product. The resolution cell definition expressed in either Equation (75) or in Equation (78) provides a useful analysis tool when determining waveform resolution performance; however, the resolution cell definition alone does not provide a complete description of resolution performance. The resolution measures  $\Delta\tau$  and  $\Delta f$  are based on independent measurements of range-time delay and frequency of the central lobe of the ambiguity function. In other words,  $\Delta\tau$  is the resolution width in  $\tau$  for a known DFS  $f_d$ , and  $\Delta f$  is the resolution width in  $f$  for a known RTD  $\tau_d$ . As Rihaczek (30:93-99) and Woodward (41:118-124) explain, when combining the two resolution measurements to form the nominal resolution cell one may conclude that any waveform with large time-bandwidth product  $TB \gg 1$  will result in a smaller resolution-cell. However, due to the amplitude constraint of Equation (43) of the ambiguity function and the volume constraint of Equation (42) of the ambiguity function, waveforms of large time-bandwidth products will necessarily exhibit ambiguities elsewhere in the  $(\tau, f)$  plane which can mask the target response of the resolution cell centered at the origin of the  $(\tau, f)$  plane.

Rihaczek introduces the term self-clutter to describe the interference of unwanted targets due to waveforms with ambiguity functions which have significant side-lobes or additional ambiguities in the form of near replicas of the central spike in the  $(\tau, f)$  plane (30:92). Therefore, radar resolution in a dense target environment must be determined in terms of the resolution cell definition and the additional ambiguities described as self-clutter which can possibly mask the resolution-cell response.

In this section, it has been shown that the MF response in a dense target environment is described statistically in terms of the target's mean backscatter cross section  $\bar{\sigma}(\bar{\tau}_d, \bar{f}_d)$  and the corresponding mean power MFSLR response. This statistical average approximation of the target backscatter and the MFLSR response is valid with the condition that the point targets do not change their orientation significantly over the pulse duration. Since the mean power MFSLR response as given in Equation (54) describes a two-dimensional convolution of the scattering function  $\bar{\sigma}(\bar{\tau}_d, \bar{f}_d)$  with the ambiguity function  $\theta(\tau, f)$ , resolution in the average RTD and average DFS is defined in terms of the central spike widths  $\Delta\tau$  and  $\Delta f$  of  $\theta(\tau, f)$ . Three radar resolution criteria which measure  $\Delta\tau$  and  $\Delta f$  of  $\theta(\tau, f)$  were given. In general, target resolution will require knowledge of both the signal ambiguity function and the statistical characteristics of the target. The next section provides a more detailed discussion of the statistical characteristics of the aerosol target.

### 3.4 Target Model

The discussion of Section 3.3 led to a statistical model of the dense target environment in terms of the target's mean cross section  $\bar{\sigma}(\bar{\tau}_d, \bar{f}_d)$ . This statistical model and the corresponding MFSLR response is valid as long as the point target distribution in  $\tau_d$  and  $f_d$  which composes the dense target does not change significantly over the pulse duration. In other words, changes in the point scatterer distribution in  $\tau_d$  and  $f_d$  must be small enough that  $\bar{\sigma}(\bar{\tau}_d, \bar{f}_d)$  is a meaningful quantity to describe the target. Since aerosol particles rapidly change their orientation on the scale of the transmitted laser wavelength, this model is valid only for short duration pulses (i.e.  $\approx 1\mu s$ ). To consider the more general case where the orientation of the aerosols changes significantly over the pulse duration, a more rigorous statistical model of the dense aerosol target is required.

As in Section 3.3, the aerosol target model can be described as a randomly distributed array of point targets which are distributed in range and velocity. Aerosol

particles of a diameter on the order of the optical signal wavelength transmitted will backscatter most of the energy received. Although some degree of molecular backscattering occurs, it is generally assumed to be negligible in comparison to the aerosol backscattering (18:67). For example, under typical clear-air atmospheric conditions, most of the energy received from a lidar transmitting at the  $10\mu m$  wavelength will be backscattered from aerosols of diameter  $1-3\mu m$  (24:450). The number density of these particles within the spatial extent of the pulse transmitted, depends on a multitude of factors such as geographic location, altitude, weather conditions, season, etc., and will typically include several thousand aerosols (25). From a theoretical point of view, one can generally assume that the lidar beam will illuminate an infinite number of point targets with a nominal separation on the order of a wavelength for  $10\mu m$  lidar (15).

From Goodman (12:347-356) one finds that when monochromatic light illuminates a rough surface (rough on the scale of the wavelength  $\lambda$ ) the reflected image has a granular appearance due to numerous bright and dark spots. This effect is commonly referred to as laser speckle. The randomly placed aerosol particles within the volume which the lidar beam illuminates individually radiate incoherent fields of random phases. At the receiver, the superposition of the fields backscattered from each of the aerosols within an illumination volume will form the resultant speckle pattern. The illumination volume of the aerosols is defined by the beam width and the spatial extent of the transmitted pulse equal to  $cT/2$  where  $T$  represents the time duration of the pulse transmitted. The received signal from a dense target such as aerosols can be expressed as

$$s_r(t) = \sum_{n=1}^{\infty} \sigma_n^{1/2} \exp(\phi_n) m(t - \tau_{dn}) \exp(j2\pi f_{dn}t) \quad (79)$$

where

$$s_r(t) = \text{complex received signal at baseband (V)}$$

$\sigma_n^{1/2}$	= reflectivity of the nth point target
$\phi_n$	= unknown phase of the nth point target (rads)
$m(t - \tau_d)$	= complex modulation signal transmitted (V)
$\tau_{dn}$	= range-time delay of the nth point target (s)
$f_{dn}$	= Doppler frequency shift of the nth point target (Hz)

From Hardesty (14:58-60), the backscattered signal  $s_r(t)$  as expressed in Equation (79) represents a superposition of the backscattered signals from each aerosol point target. The phase  $\phi_n$  of each aerosol is statistically described by a uniform distribution with the probability density function

$$p(\phi_n) = \begin{cases} \frac{1}{2\pi} & \text{if } -\pi \leq \theta_n \leq \pi \\ 0 & \text{otherwise} \end{cases} \quad (80)$$

Therefore, the backscattered signal from each aerosol point target has a random, uniformly distributed phase  $\phi_n$ , and the backscattered signal  $s_r(t)$  expressed in Equation (79) represents a superposition of the backscattered signals of random phase from each point target. As a result, for a given time  $t_1$  after signal transmission, the received signal  $s_r(t_1)$  is described statistically in terms of its amplitude and phase. The amplitude of the resultant signal  $|s_r(t)|$  is described statistically as a Rayleigh random variable (14:58-60) with the probability density function

$$p(|s_r(t_1)|) = \begin{cases} \left(\frac{|s_r(t_1)|}{2\sigma^2}\right) \exp\left[-\frac{|s_r(t_1)|^2}{2\sigma^2}\right] & |s_r(t_1)| \geq 0 \\ 0 & |s_r(t_1)| < 0 \end{cases} \quad (81)$$

where  $\sigma^2$  is the mean squared value of  $|s_r(t_1)|$ . The resultant phase of  $s_r(t_1)$  designated as  $\phi_r(t_1)$  is described statistically as a uniformly distributed random variable with the uniform probability density expressed in Equation (80).

As Hardesty and Menzies explain, if a lidar of a single carrier frequency  $f_c$  illuminates a volume of dense, randomly distributed aerosols which are stationary

with respect to each other, the resultant backscattered signal  $s_r(t)$  will consist of a sinusoidal signal of the carrier frequency  $f_c$  plus or minus the Doppler frequency-shift with a constant Rayleigh distributed amplitude and constant uniformly distributed phase. Under real atmospheric conditions, the turbulence and wind shear within the scattering volume cause the aerosols to move relative to each other. The relative aerosol motion within the scattering volume causes the aerosol particles to change their orientation with respect to the lidar receiver. As a result, the superposition of the backscattered signals change with time causing the random amplitude and random phase of  $s_r(t)$  to also change with time. Therefore,  $s_r(t)$  is described as a random process. The changes in random amplitude and random phase of  $s_r(t)$  effectively broaden the bandwidth of  $s_r(t)$  (24:453).

The temporal correlation function of  $s_r(t)$  expressed as

$$R_{s_r}(\tau) = E[s_r(t)s_r^*(t + \tau)] \quad (82)$$

provides a measure of how rapidly the received signal changes with time. If the received signal is assumed to represent a stationary random process (this representation of  $s_r(t)$  is discussed in more detail in the following paragraphs) then the Fourier transform of  $R_{s_r}(\tau_d)$  represents the power spectral density (PSD) of  $s_r(t)$ . Hardesty shows that the shape of the PSD of  $s_r(t)$  is proportional to the probability distribution of the radial wind velocities within the scattering volume (14:175-179). Hardesty and Menzies (24:453) state that the temporal correlation time  $t_c$  of the received signal which provides a measure of how rapidly  $s_r(t)$  varies with time can be expressed to a rough approximation as

$$t_c \approx \lambda/\sigma_v \quad (83)$$

where  $\lambda$  is the laser wavelength transmitted and  $\sigma_v$  is the standard deviation of the distribution of aerosol radial velocities within the scattering volume.



Chapters 11-13 of Van Trees' text (39:357-536) provide additional insight into the modeling required to adequately represent the statistical nature of the backscattered signal  $s_r(t)$  by using an alternate approach to that presented in Equation (79). Van Trees provides a general, dense target environment model which applies directly to aerosol imaging. Since the received signal consists of a large number of randomly distributed point target contributions, Van Trees also statistically models the backscattered signal as a random process with a time-varying, Rayleigh distributed amplitude and a time-varying, uniformly distributed phase. Van Trees models the target backscatter as a complex Gaussian random process  $\gamma_{DR}$  which can be expressed in terms of real and imaginary components as

$$\gamma_{DR} = \gamma_{DR_R} + j\gamma_{DR_I} \quad (84)$$

where  $\gamma_{DR_R}$  and  $\gamma_{DR_I}$  are jointly Gaussian random processes with identical covariance functions. For the dense aerosol target case, the aerosols are assumed to compose a continuous range-spread, frequency-spread, speckle target with the complex received signal expressed as

$$s_r(t) = E_t^{1/2} \int_{-\infty}^{\infty} s(t - \tau_d) \gamma_{DR}(\tau_d, t - \tau_d/2) d\tau_d \quad (85)$$

where

- $E_t$  = Transmitted energy (J)
- $s(t)$  = Complex transmitted signal (V)
- $s_r(t)$  = Sample function from a complex Gaussian random process (V)
- $\tau_d$  = Range time-delay coordinate with  $\tau_d = 2R/c$  (s)
- $\gamma_{DR}(\tau_d, t)$  = Complex Gaussian random process with independent variables  $(\tau_d, t)$  of range and time.

Physically, the mean and covariance of  $\gamma_{DR}(\tau_d, t - \tau_d/2)$  describe the statistical characteristics of the aerosol target backscatter. Van Trees makes two assumptions about

the Gaussian random process statistics of  $\gamma_{DR}(\tau_d, t - \tau_d/2)$  which are stated as follows: Assumption 1. The return from each range interval  $\Delta\tau_d$  is a sample function of a stationary, zero-mean complex Gaussian random process. Assumption 2. The returns from different range intervals  $\Delta\tau_d$  are statistically independent. As a result of Assumption 1, the mean value of  $\gamma_{DR}(\tau_d, t - \tau_d/2)$  is equal to zero. And as a result of Assumption 2, the covariance function of  $\gamma_{DR}(\tau_d, t - \tau_d/2)$  designated as  $C_\gamma(t, u)$  can be expressed as

$$C_\gamma(t, u) = E[\gamma_{DR}(\tau_d, t)\gamma_{DR}'(\tau_d', u)] = K_{DR}(\tau_d, t - u)\delta(\tau_d - \tau_d') \quad (86)$$

where the function  $K_{DR}(\tau_d, t - u)$  is dependent upon the reflective properties of the target and where the delta function  $\delta(\tau_d - \tau_d')$  is a result of the statistical independence requirement of Assumption 2.

Van Trees introduces the scattering function definition as

$$S_{DR}\{\tau_d, f_d\} = \int_{-\infty}^{\infty} K_{DR}(\tau_d, \alpha) \exp(-j2\pi f_d \alpha) d\alpha \quad (87)$$

where the scattering function  $S_{DR}\{\tau_d, f_d\}$  represents the Fourier transform of  $K_{DR}(\tau_d, \alpha)$ ; therefore,  $K_{DR}(\tau_d, \alpha)$  can be expressed as

$$K_{DR}(\tau_d, \alpha) = \int_{-\infty}^{\infty} S_{DR}\{\tau_d, f_d\} \exp(j2\pi f_d \alpha) df_d \quad (88)$$

$S_{DR}\{\tau_d, f_d\}$  represents the range-dependent PSD of the Gaussian random process  $\gamma_{DR}(\tau_d, t)$ . Since  $\gamma_{DR}(\tau_d, t)$  is a zero-mean, complex Gaussian random process,  $s_r(t)$  as expressed in Equation (85) represents a sample function from a zero-mean complex Gaussian random process. The signal  $s_r(t)$  at the receiver is completely characterized by its complex covariance function expressed as

$$C_{s_r}(t, u) = E[s_r(t)s_r^*(u)] \quad (89)$$

Substituting Equation (85) into Equation (89) yields an expression for the complex covariance function given below:

$$C_{s_r}(t, u) = E_t \int \int_{-\infty}^{\infty} s(t - \tau_d) s^*(u - \tau'_d) E[\gamma_{DR}(\tau_d, t - \tau_d/2) \gamma_{DR}(\tau'_d, t - \tau'_d/2)] d\tau_d d\tau'_d \quad (90)$$

Substitution of Equation (88) into Equation (90) yields

$$C_{s_r}(t, u) = E_t \int_{-\infty}^{\infty} s(t - \tau_d) s^*(u - \tau'_d) K_{DR}(\tau_d, t - u) d\tau_d \quad (91)$$

Substitution of  $K_{DR}(\tau_d, \alpha)$  in terms of the scattering function  $S_{DR}\{\tau_d, f_d\}$  given in Equation (87) yields an alternative expression for  $C_{s_r}(t, u)$  expressed as

$$C_{s_r}(t, u) = E_t \int \int_{-\infty}^{\infty} s(t - \tau_d) s^*(u - \tau_d) S_{DR}\{\tau_d, f_d\} \exp[j2\pi f_d(t - u)] df_d d\tau_d \quad (92)$$

Recall that  $s_r(t)$  represents the received signal at the lidar receiver prior to matched-filter processing. Equations (85) through (92) provide a summary of the model derivation Van Trees (39:357-536) developed for range-spread, frequency-spread targets which is useful in developing a scattering model for aerosols. These equations provide a complete statistical characterization of the aerosol backscattered signal. Also, these equations provide the foundation necessary for developing an aerosol target model and obtaining the statistical description of the receiver's MF response. As a specific example of an aerosol scattering function model for  $S_{DR}\{\tau_d, f_d\}$ , consider Shapiro's aerosol target model.

Shapiro (33:1-5) has developed an aerosol backscatter model consistent with the Van Trees dense target development just described in Equations (85) through (92). From the Shapiro model, the received signal from aerosol backscatter, as in Equation (85), can be expressed as

$$s_r(t) = E_t^{1/2} \int_{-\infty}^{\infty} s(t - \tau_d) \gamma_{DR}(\tau_d, t - \tau_d/2) d\tau_d \quad (93)$$

where

$$\gamma_{DR}(\tau_d, t) = \exp(-j2\pi\bar{f}_d t) \int_{-\infty}^{\infty} T(\bar{\rho}, c\tau_d/2, t - \tau_d) \xi^2(\bar{\rho}, c\tau_d/2) d\bar{\rho} \quad (94)$$

where

$$\begin{aligned} T(\bar{\rho}, \tau_d, t) &= \text{random speckle target field reflection coefficient} \\ \xi^2(\bar{\rho}, c\tau_d/2) &= \text{normalized spatial beam pattern of the transmitter and} \\ &\quad \text{back propogated local oscillator at range } c\tau_d/2 \\ \bar{\rho} &= \text{the transverse polar coordinate within the plane} \\ &\quad \text{perpendicular to the line of sight of the radar beam} \\ \bar{f}_d &= \text{the mean Doppler frequency-shift of the aerosols} \end{aligned}$$

Assuming a Gaussian distribution of aerosol relative velocities, and assuming that the returns from different spatial coefficients  $\bar{\rho}$  and different range coefficients  $\tau_d$  are statistically independent, the covariance of  $T(\bar{\rho}, \tau_d, t)$  can be expressed as

$$E [T(\bar{\rho}, \tau_d, t) T^*(\bar{\rho}', \tau_d', u)] = \frac{\lambda^2}{\pi} \beta\left(\frac{c\tau_d}{2}\right) \delta(\bar{\rho} - \bar{\rho}') \delta(\tau_d - \tau_d') \exp \left[ -\frac{(t - u)^2}{t_c^2} \right] \quad (95)$$

where

$$\begin{aligned} \beta(c\tau_d/2) &= \text{aerosol backscatter coefficient at range } R = c\tau_d/2 \text{ (m}^{-1}\text{sr}^{-1}\text{)} \\ t_c &= \text{coherence time approximated by Equation (83) (s)} \end{aligned}$$

Substituting Equations (94) and (95) into Equation (86) and solving for  $K_{DR}(\alpha, \tau_d)$  yields

$$K_{DR}(\tau_d, \alpha) = \frac{\lambda^2}{\pi} \beta\left(\frac{c\tau_d}{2}\right) \left| \xi\left(\bar{\rho}, \frac{c\tau_d}{2}\right) \right|^4 \exp \left[ -\frac{\alpha^2}{t_c^2} - j2\pi\bar{f}_d \right] \quad (96)$$

Therefore, the scattering function using Equation (87) can be expressed as

$$S_{DR}\{\tau_d, f_d\} = \frac{\lambda^2}{\pi^{1/2}} \beta\left(\frac{c\tau_d}{2}\right) \left| \xi\left(\bar{\rho}, \frac{c\tau_d}{2}\right) \right|^4 t_c \exp \left[ -\pi^2 t_c^2 (f_d - \bar{f}_d)^2 \right] \quad (97)$$

Van Trees (39:361) defines the mean Doppler shift  $\bar{f}_d$  as

$$\bar{f}_d = \frac{1}{2\sigma^2} \int_{-\infty}^{\infty} f_d S_{DR}\{\tau_d, f_d\} df_d \quad (98)$$

where

$$2\sigma^2 = K_{DR}(\tau_d, 0) \quad (99)$$

The scattering function  $S_{DR}(\tau_d, f_d)$  describes the aerosol range-spread backscatter characteristics in terms of the aerosol backscatter coefficient  $\beta(c\tau_d/2)$ , and the frequency-spread backscatter characteristics in terms of a Gaussian distribution function. Note that the smaller the coherence time, the broader the frequency spread and therefore the broader the velocity distribution of the particles imaged. Also note that the Gaussian distribution term of the scattering function is centered on the mean Doppler frequency-shift  $\bar{f}_d$ . The mean Doppler frequency-shift will vary as the pulse propagates through the atmosphere and so will the coherence time as the pulse enters regions of increasing or decreasing turbulence or wind shear. The stationarity of the process is limited; therefore, this model is valid over a limited observation time.

When considering the complete description of all the point targets which the lidar pulse encounters during its propagation through the atmosphere, the overall target is seen to consist of a continuous distribution of point target velocities and ranges. The range can be considered to extend beyond the maximum range of the lidar, and the frequency will range from zero to plus or minus the highest Doppler frequency-shift due to wind velocities encountered. For a mean radial wind velocity range of 0 to  $\pm 40\text{m/s}$  the mean Doppler frequency-shift range is from 0 to  $\pm 8\text{MHz}$ .

In this section, the signal  $s_r(t)$  backscattered from a dense array of aerosols has been modeled as a zero mean, complex Gaussian random process. The aerosol scattering function  $S_{DR}\{\tau_d, f_d\}$  represents the range dependent PSD of the random process. The Shapiro aerosol model for  $S_{DR}\{\tau_d, f_d\}$  represents a specific example of

aerosol dense target modeling which is consistent with the Van Trees dense target development. Radar measurements of  $S_{DR}\{\tau_d, f_d\}$  yield the parameters of interest such as mean backscatter power, mean Doppler frequency-shift, and Doppler frequency-shift spread. Thus far only the backscattered signal  $s_r(t)$  at the radar receiver has been statistically modeled. The next logical step in the development of matched-filter aerosol sensing is a statistical description of the matched-filter radar receiver response to the backscattered signal  $s_r(t)$ .

### 3.5 Conventional Radar Receiver

As suggested in Section 3.2, the MF bank receiver response to the signal  $s_r(t)$  can be expressed as the cross-correlation with the time-translated, frequency-shifted version of the transmitted signal. The discussion of resolution in Section 3.3 led to the Rihaczek conclusion that the only means of describing the MF response in a dense target environment of randomly distributed point targets, is through the average power response of the matched filter. The average power response was shown to result in a two-dimensional convolution of the average target cross section in range and Doppler with the signal ambiguity function  $\theta(\tau, f)$ . In Section 3.4 a more detailed statistical description of the aerosol target was provided. The text of Van Trees offered a general model to describe the statistics of the aerosol target, and a specific aerosol scattering function from Shapiro was compared to the Van Trees model. For both the Rihaczek model and the VanTrees model, the mean power response of the MF represents the measureable quantity available to describe the aerosol target. Recall the output of the MFSLR as illustrated in Figure 3 can be expressed analytically as

$$|y(\tau, f)|^2 = \left| \int_{-\infty}^{\infty} s_r(t) s^*(t - \tau) \exp(-j2\pi ft) dt \right|^2 \quad (100)$$

where  $s_r(t)$  is now the aerosol backscattered signal of Equation (85). The derivation to determine the mean of Equation (100) is provided in Appendix A. This derivation

shows that the mean MFSLR response can be expressed as

$$E[|y(\tau, f)|^2] = N_o \cdot E_t \int \int_{-\infty}^{\infty} S_{DR}\{\tau_d, f_d\} \theta(\tau - \tau_d, f - f_d) df_d d\tau_d \quad (101)$$

where

- $f_d$  = target Doppler frequency shift coordinate (Hz)
- $\tau_d$  = target range-time delay coordinate (s)
- $f$  = MFSLR frequency coordinate (s)
- $\tau$  = MFSLR range-time delay coordinate (s)
- $N_o$  = mean Gaussian spectral density (W/Hz)

The mean power response of the MFSLR from Equation (101) represents a two dimensional convolution of the scattering function  $S_{DR}\{\tau_d, f_d\}$  with the ambiguity function  $\theta(\tau, f)$ . Recall from Section 3.3 the comparable result for the dense target, MFSLR response which Richaczek models as a two dimensional convolution of the mean target cross section  $\bar{\sigma}(\bar{\tau}_d, \bar{f}_d)$  with the ambiguity function  $\theta(\tau, f)$ . Thus for either case,  $\theta(\tau, f)$  along with the target model, determine radar resolution. Both  $\bar{\sigma}(\bar{\tau}_d, \bar{f}_d)$  and  $S_{DR}\{\tau_d, f_d\}$  represent PSDs associated with the backscatter from a dense array of point targets randomly distributed in range and velocity. For short time duration pulses (i.e.  $\approx 1\mu s$ ), where  $\bar{\sigma}(\bar{\tau}_d, \bar{f}_d)$  is valid, the two models should yield the same analytical results in terms of the MFSLR response.

Analytically modeling the aerosol target backscatter with the scattering function  $S_{DR}\{\tau_d, f_d\}$  provides the advantage of statistically describing the aerosol backscatter independently from the time duration of the transmitted signal. Thus the derivation of the MFSLR response of Equation (101) with the scattering function  $S_{DR}\{\tau_d, f_d\}$  represents a more general solution where the time duration of the pulse can exceed the coherence time of the aerosol target. Radar resolution in terms of Equation (101) is analogous to the radar resolution discussed in Section 3.3 in terms of the Richaczek dense target model. Thus one can think of  $S_{DR}\{\tau_d, f_d\}$  as a two

dimensional input,  $\theta(\tau, f)$  as the impulse response of a two dimensional filter, and  $E[|y(\tau, f)|^2]$  as the two dimensional filter response. Thus, the resolution with which the radar measures  $S_{DR}\{\tau_d, f_d\}$  is dependent upon the volume distributions of both  $S_{DR}\{\tau_d, f_d\}$  and  $\theta(\tau, f)$ . This volume distribution aspect of radar resolution is discussed in more detail in Chapter 4. One can compare the range and frequency resolution of a matched-filter radar receiver to the resolution achieved with current lidar systems employing Fourier spectral analysis.

As discussed in Section 2.4, current lidar systems employ Fourier spectral processing techniques to obtain estimates of a range-resolved power spectral density called a periodogram. If samples of the MFSLR output are taken across the frequency band for a single range time corresponding to  $t = \tau_d$ , an estimate of the PSD of the aerosol target is formed. The processing described is comparable to the current spectral processing technique discussed in Section 2.4. This single estimate at  $\tau_d$  is range-resolved according to the resolution width  $\Delta\tau$  of the ambiguity function  $\theta(\tau, f)$ . The range of particles which significantly contribute to the single PSD estimate at  $t = \tau_d$  for a simple rectangular pulse are contained within a range swath of width approximately

$$\Delta R \simeq \frac{c}{2B} \simeq \frac{cT}{2} \quad (102)$$

This description of range width or resolution is comparable to the range weighting function discussed in meteorological radar literature (11:52-56). In general, many pulses will be noncoherently integrated over the time duration for which the Gaussian random process is stationary. Resolution of the PSD estimate is determined in terms of the ambiguity function's frequency resolution width  $\Delta f$ . For the simple rectangular pulse,  $\Delta f \simeq 1/T$ .

Note the distinction made between resolution performance in terms of the PSD estimate of  $S_{DR}\{\tau_d, f_d\}$  and the resolution performance in terms of resolving a single point target. In general, single aerosol point targets are too dense to resolve



individually, but if the resolution definition is in terms of resolution with respect to a single point target, the convolution operation of Equation (101) on the frequency axis must be performed. However if resolution is defined in terms of the resolution with which  $S_{DR}\{\tau_d, f_d\}$  is measured, the widths  $\Delta\tau$  and  $\Delta f$  of the ambiguity function will determine waveform resolution performance. An example will illustrate the distinction.

Suppose as in Section 3.3, that the ambiguity function can be ideally represented as the impulse function

$$\theta(\tau, f) = \delta(\tau, f) \quad (103)$$

Substituting Equation (103) into Equation (101) yields the expression

$$E[|y(\tau, f)|^2] = E_t S_{DR}\{\tau, f\} \quad (104)$$

The form of Equation (104) provides the exact representation of the scattering function with infinitesimal resolution. However, if resolution is defined in terms of a single point target, then resolution in frequency will be in terms of the width in  $f$  of the scattering function  $S_{DR}\{\tau, f\}$  while resolution in range is determined by the width of the ambiguity function across the  $\tau$  axis. This statement is true as long as the MFSLR response is not coupled in frequency and range. If coupling occurs between target range and Doppler (for example, linear frequency modulated (FM) pulses), the degree of frequency spread of the scattering function along with the ambiguity function will determine resolution for both frequency and range. In the next chapter, signal waveform resolution performance for various types of radar signals will be determined in terms of the scattering function  $S_{DR}\{\tau_d, f_d\}$ .

## IV. Findings and Observations

### 4.1 Introduction

As stated previously, the primary purpose of this thesis effort is to compare the resolution performance of a conventional matched-filter radar receiver for various signal waveforms in a dense target environment such as aerosols. It is clear from the derivations of Chapter 3 that resolution in a dense target environment is determined in terms of both the scattering function and the ambiguity function. In general, the backscatter function from Dr. Shapiro which was discussed briefly in Section 3.4 is assumed to adequately represent the aerosol scattering function  $S_{DR}\{\tau_d, f_d\}$ . In this model, the target is continuous in range extending beyond the far field range of the lidar with a reflection coefficient determined by the beamwidth and the aerosol backscatter coefficient  $\beta_s(c\tau_d/2)$ . The relative velocities of the aerosols is modeled in terms of a Gaussian distribution in frequency whose width is described by the coherence time  $t_c$ . The coherence time in terms of relative aerosol velocities is approximately expressed as in Section 3.3 as  $t_c \approx \lambda/\sigma_v$ . The mean Doppler frequency  $\bar{f}_d$  of the aerosols will range from zero to the highest expected atmospheric velocities. Resolution performance in terms of the radar ambiguity function provides a measure of the resolution of the scattering function which the waveform can achieve.

The development of radar since the early 40's has resulted in a myriad of signal waveforms and signal processing techniques, and a detailed discussion of each is well beyond the scope of this paper. Fortunately however, signal waveforms may be classified in terms of their respective ambiguity function shapes into four distinct classes (31:1078-1083).

Class 1 waveforms are single pulses of carrier frequency  $f_c$  which form an ambiguity function with its volume concentrated in a central ridge at the origin of the  $(\tau, f)$  plane with low sidelobes. Class 2 waveforms also have a concentrated

volume with low sidelobes; however, the volume is skewed in the  $(\tau, f)$  plane. Single pulses with linear frequency modulation (FM) referred to as "chirp" pulses represent Class 2 waveforms, and their ambiguity function is often called the "knife edge" ambiguity function. Class 3 signals have an ambiguity function commonly referred to as the "thumbtack" ambiguity function. A large variety of signal waveforms often referred to as noise or pseudonoise waveforms which require random phase or frequency coding can be classified as Class 3 waveforms. In addition, single pulse waveforms with smoothly varying phase modulation such as quadratic FM form an approximate thumbtack ambiguity function. The distinctive characteristic of Class 3 waveforms is the narrow central spike of negligible ambiguity volume and the broad pedestal of large  $B \times T$  dimensions which contains most of the volume of the ambiguity function. Class 4 signals have an ambiguity function commonly referred to as the "bed of nails". Periodic pulse trains uniformly spaced in time represent Class 4 waveforms. Table 1 provides a summary of the more salient features of each class of waveform. The four classes of waveforms designated as Classes 1, 2, 3, and 4 are discussed in Sections 4.2 through 4.5 respectively. With these four classifications of signal waveforms in terms of their respective ambiguity function volume distributions, the task at hand is to analyze each class of waveform with respect to its resolution performance in the aerosol, dense target environment.

Table 1. Ambiguity Function Parameters (31:1080)

Radar Signals	Class 1	Class 2	Class 3	Class 4
Ambiguity function	ridge	sheared ridge	thumbtack	bed of nails
Resolution cell size	unity	unity	$1/TB$	$1/TB$
Ambiguities	no	$(\tau_d, f_d)$ coupling	no	spikes
Sidelobes	low	low	high	low
TB product	unity	$TB \gg 1$	$TB \gg 1$	$TB \gg 1$

#### 4.2 Class 1 Radar Signals

The single radar pulse of carrier frequency  $f_c$  represents Class 1 radar waveforms. The normalized rectangular pulse is expressed in complex baseband form as

$$s_t(t) = \frac{1}{T^{1/2}} \text{rect}\left(\frac{t}{T}\right) \quad (105)$$

where  $T$  represents the time duration of the pulse. The ambiguity function of the rectangular pulse is derived from the ambiguity function definition of Section 3.2, Equation (26) and is expressed as

$$\chi(\tau, f) = \begin{cases} \left(1 - \frac{|\tau|}{T}\right) \text{sinc}\left[\left(1 - \frac{|\tau|}{T}\right) T f\right] & \text{if } |\tau| \leq T \\ 0 & \text{if } |\tau| > T \end{cases} \quad (106)$$

where the function  $\text{sinc}(x) = (\sin \pi x)/(\pi x)$ . If the function  $\text{tri}(\tau)$  is defined as

$$\text{tri}(\tau) = \begin{cases} \left(1 - \frac{|\tau|}{T}\right) & \text{if } |\tau| \leq T \\ 0 & \text{if } |\tau| > T \end{cases} \quad (107)$$

then the ambiguity function of Equation (106) can be simplified to

$$\chi(\tau, f) = \text{tri}(\tau) \text{sinc}[(T f) \text{tri}(\tau)] \quad (108)$$

Therefore, the squared-modulus ambiguity function  $\theta(\tau, f)$  is expressed as

$$\theta(\tau, f) = \text{tri}^2(\tau) \text{sinc}^2[(T f) \text{tri}(\tau)] \quad (109)$$

The common, two-dimensional contour plot of the ambiguity function  $\theta(\tau, f)$  is shown in Figures 4 and 5 for long and short time duration pulses respectively. The elliptical regions enclose the areas where the height of  $\theta(\tau, f)$  is significant while lightly shaded regions depict the areas where the height of  $\theta(\tau, f)$  is small but nonzero. The ellipses of Figures 4 and 5 represent the approximate borders

of the half-power, equal height contours of  $\theta(\tau, f)$ . The ellipse which composes the half-power border consists of all the points of  $(\tau, f)$  which satisfy the equation  $\theta(\tau, f) \simeq 1/2$ . This convention for two-dimensional contour plots introduced by Siebert (35:217) simplifies the analysis of various waveforms and is common to many radar texts (38, 26, 39). For the rectangular pulse ambiguity function of Equation (109), the shape of  $\theta(\tau, f)$  along the  $\tau$  and  $f$  axes are expressed respectively as

$$\theta(\tau, 0) = \text{tri}^2(\tau) \quad (110)$$

$$\theta(0, f) = \text{sinc}^2(Tf) \quad (111)$$

As shown in Section 3.3, the range time-delay (RTD) and Doppler frequency-shift (DFS) resolution widths for the rectangular pulse are respectively given as

$$\Delta\tau \simeq T \quad (112)$$

$$\Delta f \simeq \frac{1}{T} \quad (113)$$

Combining Equations (112) and (113) forms the nominal resolution cell expressed as

$$\Delta\tau\Delta f \simeq 1. \quad (114)$$

Similar results apply for the Gaussian pulse case. The normalized Gaussian pulse expressed in complex baseband form is

$$s_t(t) = \left(\frac{1}{\pi T^2}\right)^{1/4} \exp\left(-\frac{t^2}{2T^2}\right) \quad (115)$$

where  $T$  is the root-mean-square (RMS) time duration for the signal. Derivation of the Gaussian signal ambiguity function yields

$$\chi(\tau, f) = \exp\left[-\left(\frac{\tau^2}{4T^2} + \pi^2 T^2 f^2\right)\right] \quad (116)$$

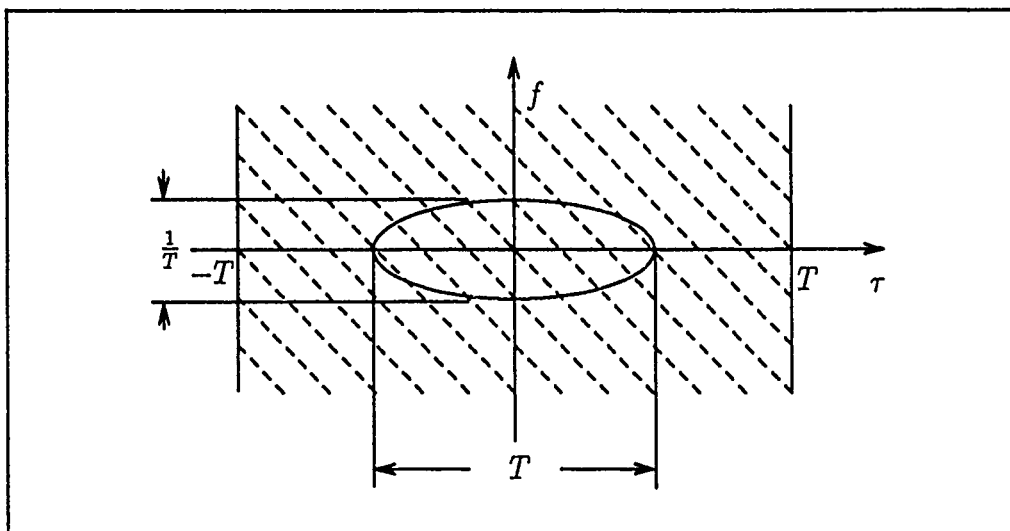


Figure 4. Contour Plot of a Class 1 Ambiguity Function (Long Pulse) (35:217)

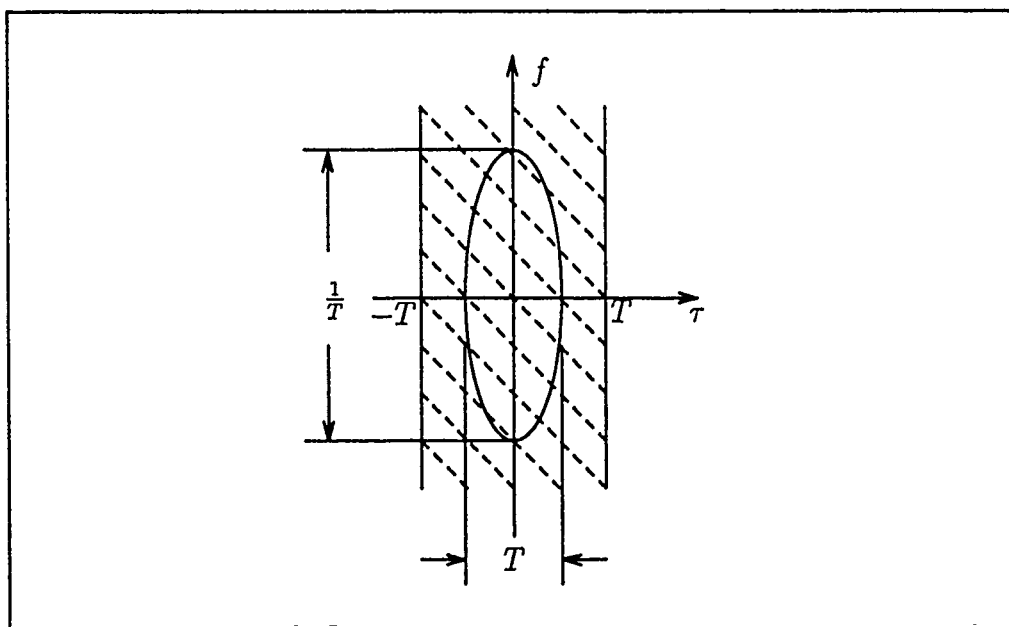


Figure 5. Contour Plot of a Class 1 Ambiguity Function (Short Pulse) (35:217)

Therefore, the squared-modulus ambiguity function  $\theta(\tau, f)$  can be expressed as

$$\theta(\tau, f) = \exp \left[ - \left( \frac{\tau^2}{2T^2} + 2\pi^2 T^2 f^2 \right) \right] \quad (117)$$

As in the rectangular pulse case, the equal height contours of  $\theta(\tau, f)$  form ellipses, and the half-power ellipse of the Gaussian pulse is comparable to the half-power ellipses of Figures 4 and 5. The shape of  $\theta(\tau, f)$  along the  $\tau$  and  $f$  axes provides a measure of RTD and DFS resolution. For the Gaussian pulse, the shape of  $\theta(\tau, f)$  along both axes is Gaussian.

Due to the Fourier transform relationship between the time and frequency domains, to a close approximation, the bandwidth  $B$  of any Class 1 waveform is equal to the reciprocal of the time duration  $T$ . Therefore, Class 1 waveforms always have nominal resolution cells which have the approximate dimensions of  $B \times T$  with an approximate area of unity. Figures 4 and 5 illustrate the basic concept. Figure 4 represents the ambiguity function for a long time duration pulse, and Figure 5 illustrates the ambiguity function of a short time duration pulse. As these two figures illustrate, an increase in time duration  $T$  results in a decrease in the size of the frequency resolution dimension  $\Delta f$ . If the time duration  $T$  is increased to infinity, the signal becomes a continuous wave signal with infinitesimal frequency resolution and with no range resolution. Conversely, if the pulse is infinitesimally small in time duration, the impulse will provide infinitesimal range resolution with no frequency resolution.

The coordinate transformations to the resolution widths in range and radial velocity are respectively expressed as

$$\Delta \tau = \frac{c \Delta R}{2} \quad (118)$$

$$\Delta f = \frac{2 \Delta V_r}{\lambda} \quad (119)$$

Substitution of Equations (118) and (119) into Equation (114) will yield the nominal range-velocity resolution cell given as

$$\Delta R \Delta V_r = \frac{c\lambda}{4} \quad (120)$$

For  $c = 3 \times 10^8$  and  $\lambda = 10\mu m$ ,  $\Delta R \Delta V_r = 750m^2/s$ . As Equation (120) illustrates, the only means of reducing the nominal range-velocity resolution cell of a Class 1 waveform is to reduce the carrier wavelength. For the simple Class 1 radar signal, the resolution cell defined by Equation (120) provides an accurate and complete description of the resolution with which the radar measures the aerosol scattering function  $S_{DR}\{\tau_d, f_d\}$ . In other words, the mean MFSLR response measures the aerosol scattering function with the resolution in range and radial velocity of the nominal resolution cell regardless of the distribution of  $S_{DR}\{\tau_d, f_d\}$ . The radar resolution of the other three classes of radar signal depend on the volume distributions of both  $S_{DR}\{\tau_d, f_d\}$  and  $\theta(\tau, f)$  over the  $(\tau, f)$  plane. The remaining three classes of radar signals to consider are called pulse compression signals. These large time-bandwidth product signals may improve resolution dependent upon the target scattering function characteristics. Recall from Section 3.2 that the total volume of  $\theta(\tau, f)$  remains fixed. Pulse compression radar signals simply redistribute the fixed ambiguity volume. The first class of pulse compression signals designated as Class 2 radar signals achieve large time-bandwidth products through frequency modulation.

### 4.3 Class 2 Radar Signals

Single pulses with linear frequency modulation (FM) represent Class 2 signals. This radar signal is commonly referred to in the radar literature as a chirp pulse, and radars which implement them are often called chirp pulse compression radars. The technique of chirp pulse compression has been used extensively since its development in the 40's, and the literature describing its features abounds (38, 26, 39, 30). As Skolnik explains (38:420-423), chirp pulse compression provides the radar designer



the means of using a long time duration pulse to achieve large radiated energy while still achieving the range resolution of a short duration pulse. In addition, means of acquiring accurate range and velocity information from multiple pulses have been developed.

A linear FM chirp pulse can be generated by either active or passive generation techniques. The active generation technique requires direct time-domain frequency modulation of the radar transmitter. For a rectangular pulse of constant amplitude  $A$  and time duration  $T$  as illustrated in Figure 6a, the frequency modulation is linear over the time duration  $T$  of the pulse as illustrated in Figure 6b. The slope  $|k|$  of the linear FM can be expressed as

$$|k| = B/T \quad (121)$$

where the bandwidth  $B$  from Figure 6b is given as  $B = f_2 - f_1$  and where  $T$  is the time duration of the pulse. The slope  $k$  in general can be positive or negative.

The passive generation technique requires an impulse function or short time duration pulse as the input to a dispersive phase filter. The frequency transfer function  $H(f)$  of the dispersive phase filter can be expressed in general as

$$H(f) = |H(f)| \exp [j\theta(f)] \quad (122)$$

where the magnitude of the transfer function  $|H(f)|$  is constant and the phase of the transfer function  $\theta(f)$  is a quadratic function of  $f$ . In general, the impulse response of a dispersive filter with a quadratic phase function produces an output signal whose time domain phase is also quadratic and thus whose frequency varies linearly with time. The response of the dispersive phase filter to a short time duration signal with large bandwidth  $B$  is a long time duration signal with the bandwidth  $B$  of the short pulse. The quadratic phase of the time domain signal output from the filter is equivalent to linear frequency modulation as in the active generation technique

discussed previously. Either the active or the passive generation technique forms an approximately equivalent linear FM signal (30, 38). For the purpose of comparing the resolution performance, either generation technique will yield equivalent results.

Consider the active generation case. The transmitted chirp pulse can be written in general, complex baseband form as

$$s(t) = |s(t)| \exp(j\pi kt^2) \quad (123)$$

where the magnitude  $|s(t)|$  is a constant  $A$  as shown in Figure 6a, and the phase is quadratic which is equivalent to the linear FM slope of Figure 6b with  $k = B/T$ . The instantaneous frequency of  $s(t)$  is  $f(t) = kt$ .

For the analysis to follow, a detailed description of the spectrum of the signal  $s(t)$  of Equation (123) is unnecessary. The Fourier transform of the general chirp pulse of Equation (123) can be written in general form as

$$S(f) = |S(f)| \exp[j\theta(f)] \quad (124)$$

where  $\theta(f)$  is a quadratic function of frequency and the shape of  $|S(f)|$  is a function of both the envelope of the transmitted signal and the bandwidth  $B$  representing the degree of linear frequency modulation (30, 3). If the time-bandwidth product  $TB$  of the transmitted signal is large ( $TB \gg 1$ ), it can be shown that the bandwidth of the spectrum envelope is approximately the linear FM modulation bandwidth  $B$  where  $B = f_2 - f_1$  as shown in Figure 6b (38:423). Often  $B$  is called the chirp bandwidth. Thus the transmitted chirp pulse has an envelope of time duration  $T$  and an increased bandwidth of approximately  $B$ .

To compress the pulse in the time domain, a matched filter is employed. The frequency transfer function can be expressed in general as

$$H(f) = S^*(f) = |S(f)| \exp[-j\theta(f)] \quad (125)$$

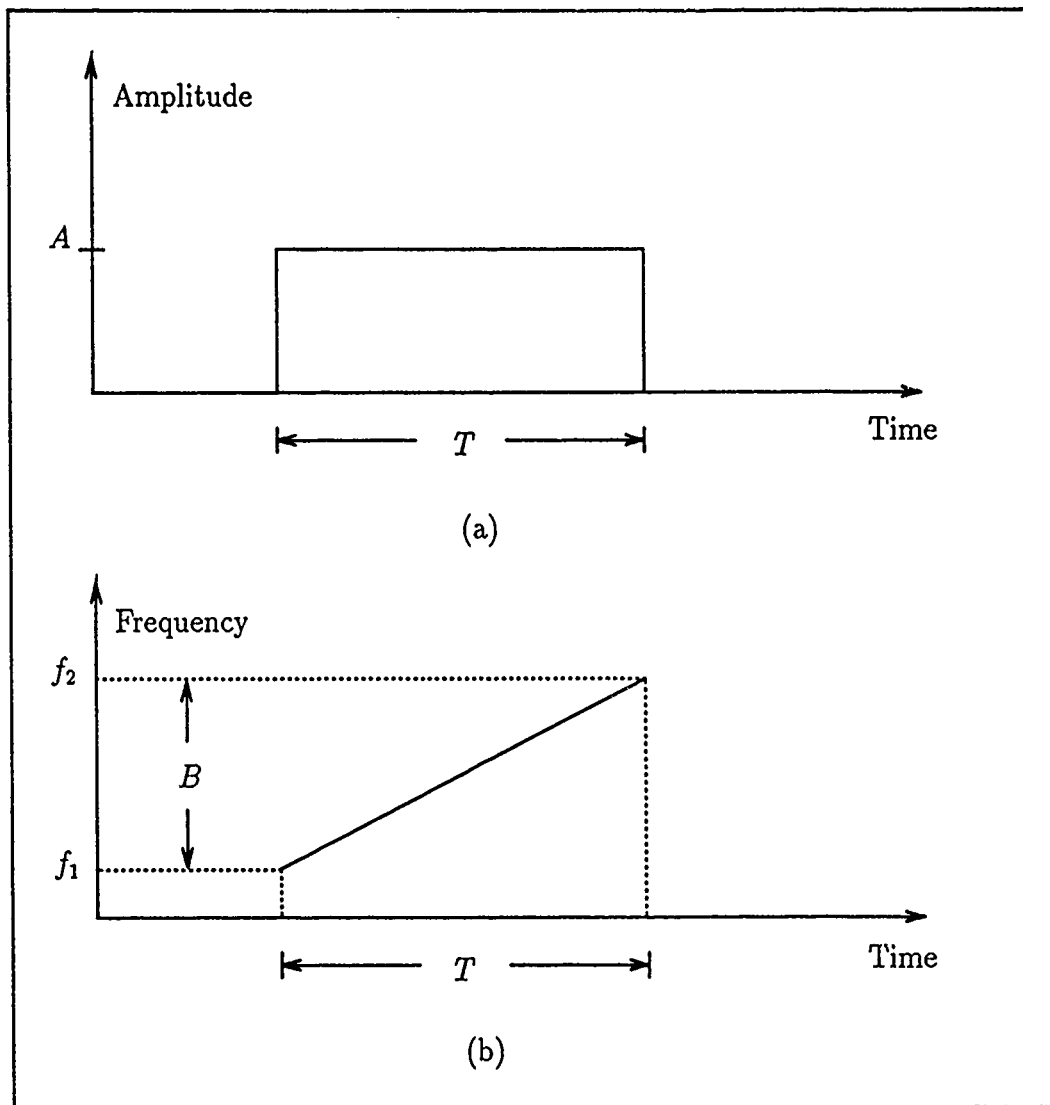


Figure 6. Amplitude (a) and Frequency (b) of the Transmitted Chirp Pulse (38:423)

where the transfer function  $H(f)$  is the complex conjugate of the transmitted signal spectrum written in general form in Equation (124). Thus the matched-filter is represented as a dispersive phase filter with the quadratic phase characteristic  $-\theta(f)$ . As a result, the filter removes the nonlinear phase  $\theta(f)$  of the received signal and compresses the received signal into a short duration pulse. The degree of compression of the MF response is proportional to the bandwidth  $B$ . Although a large time-bandwidth signal is transmitted, the MF response compresses the time duration to form a pulse of duration  $1/B$  with a bandwidth of  $B$ ; thus, the MF response produces a signal with a time-bandwidth product of unity ( $TB \simeq 1$ ) (30:55). Derivation of the chirp pulse ambiguity function will provide a more precise description of the chirp pulse MF response.

Consider the active generation of a rectangular-envelope, chirp pulse. The transmitted signal can be written in normalized, complex baseband form as

$$s(t) = \frac{1}{T^{1/2}} \text{rect}\left(\frac{t}{T}\right) \exp(j\pi k t^2) \quad (126)$$

Similarly, the Gaussian-envelope transmitted signal can be written in normalized complex baseband form as

$$s(t) = \left(\frac{1}{\pi T^2}\right)^{1/4} \exp\left[\left(\frac{1}{2T^2} + j\pi k\right) t^2\right] \quad (127)$$

where  $T$  is the RMS signal time duration. The rectangular and Gaussian envelope pulses represent the two most common pulses shapes considered in radar texts. The Gaussian chirp pulse yields a slightly broader MF response without significant sidelobes as compared to the rectangular chirp pulse. For both these pulses, the linear FM ambiguity functions are similar in form and interpretation, so only the rectangular pulse ambiguity function is analyzed in detail.

One of the properties of the ambiguity function (39:290) can be stated as follows: If

$$s(t) \leftrightarrow \chi(\tau, f) \quad (128)$$

where the symbol " $\leftrightarrow$ " means "has the ambiguity function", then

$$s(t) \exp(j\pi kt^2) \leftrightarrow \chi(\tau, f - k\tau) \quad (129)$$

Therefore, the ambiguity function of the chirp pulse is simply the ambiguity function of the unmodulated pulse of the same time duration with its major axis rotated to the slope of  $f = k\tau$  as illustrated with a two-dimensional contour plot of  $\theta(\tau, f)$  in Figure 7. Substituting the expression for the ambiguity function of the unmodulated rectangular pulse in Equation (108) into Equation (129), the chirp pulse ambiguity function can be written as

$$\chi(\tau, f) = \text{tri}(\tau) \text{sinc}[T(f - k\tau)\text{tri}(\tau)] \quad (130)$$

where again  $|k| = B/T$ . From the definition of the sinc function, Equation (130) can be expressed as

$$\chi(\tau, f) = \frac{\sin[\pi T(f - k\tau)\text{tri}(\tau)]}{\pi T(f - k\tau)} \quad (131)$$

For large time-bandwidth product signals ( $TB \gg 1$ ), the  $\text{tri}(\tau)$  term in the numerator of Equation (131) represents a slowly varying distortion term which can be ignored (30:171). Therefore, the approximate envelope of the ambiguity function is expressed as

$$\chi(\tau, f) \simeq \text{sinc}[\pi T(f - k\tau)] \quad (132)$$

Thus the squared-modulus ambiguity function  $\theta(\tau, f)$  is given in approximate form as

$$\theta(\tau, f) \simeq \text{sinc}^2[\pi T(f - k\tau)] \quad (133)$$

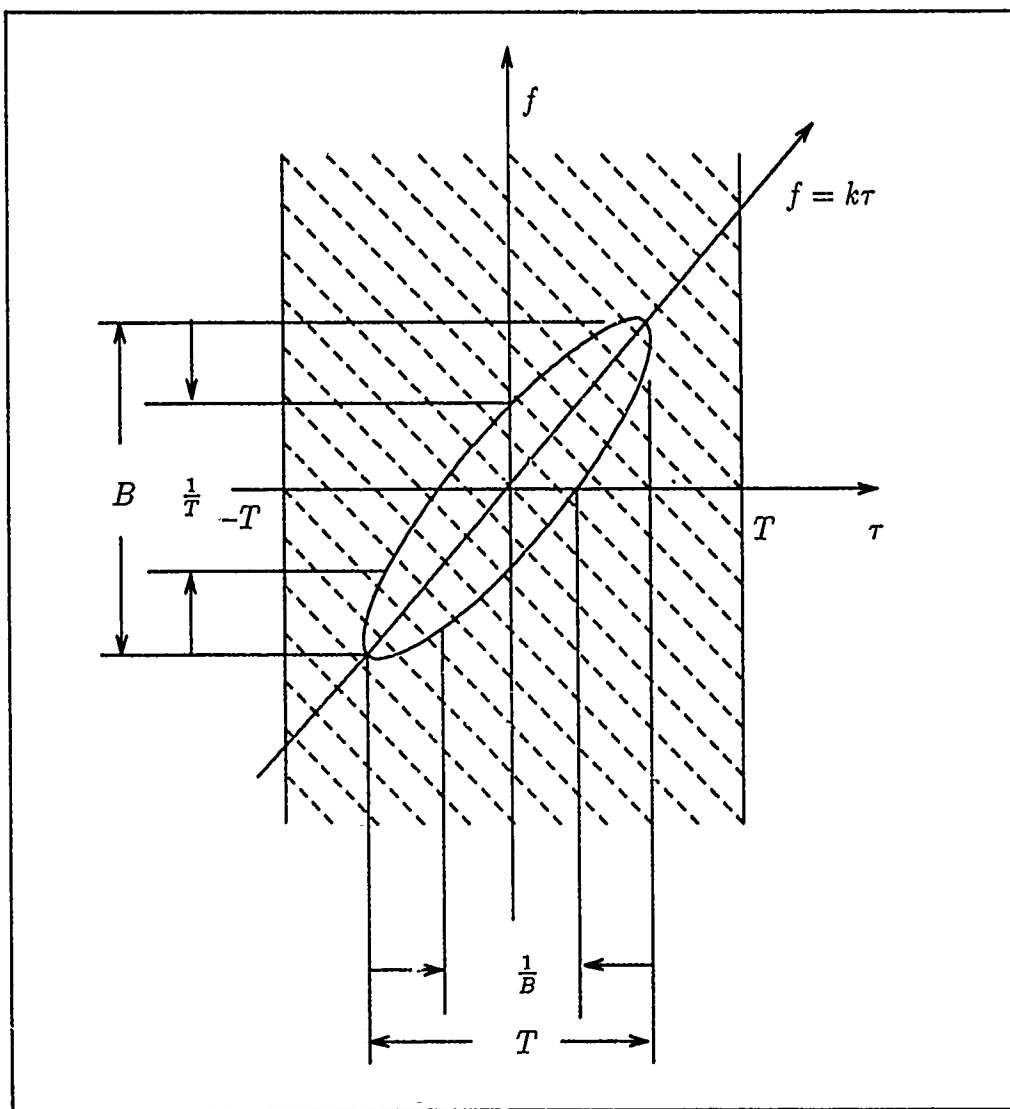


Figure 7. Contour Plot of a Class 2 Ambiguity Function (35:217)

Equations (132) and (133) illustrate the symmetry of the ambiguity function in  $\tau$  and in  $f$ . A vertical slice parallel to either axis yields a sinc function MF response. This symmetry indicates the coupling effect between target range and velocity for chirp pulse compression radar. Recall from Section 3.2 that the ambiguity function represents the response of an array of MFs shifted in frequency. An alternative view of the ambiguity function is also possible. The ambiguity function also represents the response of a single MF as the Doppler frequency of the received signal is varied (38:411-412). Due to the symmetry of Equations (132) and (133), the MF response for a Doppler mismatch  $f_d$  is equivalent to the MF response translated by  $\Delta\tau_d = f_d/k$  for  $f_a = 0$ . As a result, a MF receiver for the linear FM chirp pulse employs a single MF. This technique is possible since Doppler frequency shifts within the broad bandwidth  $B$  of the filter simply produce an additional time lead or time lag ( $\Delta\tau_d = f_d/k$ ) on the  $\tau$  axis dependent upon the slope of  $k$  employed with limited amplitude attenuation or distortion (30:248).

For the single MF case, letting  $f = 0$  in Equation (133) yields the MF response on the  $\tau$  axis expressed as

$$\theta(\tau, 0) = \text{sinc}^2(\pi T k \tau) \quad (134)$$

Substituting  $k = B/T$  into Equation (134) yields

$$\theta(\tau, 0) = \text{sinc}^2(\pi B \tau) \quad (135)$$

Therefore as discussed previously, the single MF response of Equation (135) compresses the received signal to a time duration of  $1/B$  with the broad bandwidth  $B$ . As a result, the large time-bandwidth product of the received signal is compressed in time to a MF output signal with  $TB \simeq 1$ .

In summary, the MF receiver for linear FM chirp pulses consists of a linear FM frequency characteristic which is opposite to the frequency characteristic of the transmitted chirp pulse. The receiver compresses the received signal from a time

duration  $T$  to a time duration  $1/B$  with a bandwidth of  $B$ . The MF output is a compressed signal with  $TB \simeq 1$ . The chirp pulse receiver can employ a single MF since a Doppler frequency shift of the received signal within the bandwidth  $B$  of the filter produces an additional time lead or time lag in the MF response given as  $\Delta\tau_d = f_d/k$  which is dependent upon the slope of  $k$  of the transmitted signal with limited attenuation or distortion.

The time-frequency coupling of the linear FM signal allows a considerable simplification of the radar receiver since only one MF is required. However, since both the target's range and the target's radial velocity cause delays in the MF response, the receiver's simplicity also results in a limitation of the receiver's ability to determine both target range and radial velocity simultaneously from one pulse. In fact, this receiver achieves no resolution in Doppler frequency shift within the bandwidth  $B$ .

Before resolution properties of the linear FM signal are discussed, first consider the simple case where the radar images a single point target of unknown RTD  $\tau_d$  and unknown DFS  $f_d$ . As a result of the target DFS  $f_d$ , the output peak  $\tau_p$  of the MF response occurs at

$$\tau_p = \tau_d + \Delta\tau_d \quad (136)$$

where  $\Delta\tau_d = f_d/k$ . Thus, for a moving target, the peak of the MF response does not represent the true target range  $\tau_d$ . The symmetry of Equations (132) and (133) shows that all point targets with combinations of  $\tau_d$  and  $f_d$  which lie along the ridge of the ambiguity function satisfy the following equation:

$$f_d - k\tau_d = 0 \quad (137)$$

All combinations of  $(\tau_d, f_d)$  which satisfy Equation (137) will produce a peak at the same location  $\tau_p$ . Therefore, the range measurement  $\tau_p$  is ambiguous over the time duration  $T$  of the chirp pulse. Klauder (21:804) and Rihaczek (30:246-248) show that



there is a technique called "range extrapolation" which resolves the range ambiguity inherent to a chirp pulse compression receiver imaging a single point target. As Rihaczek explains, if the point target DFS  $f_d$  is converted to the radial velocity coordinate  $V_r$ , the range error due to  $\Delta\tau_d$  can be expressed as

$$\Delta R = (\Delta\tau_d) \left( \frac{c}{2} \right) = \left( \frac{f_d}{k} \right) \left( \frac{c}{2} \right) = \left( \frac{2V_r}{k\lambda} \right) \left( \frac{c}{2} \right) = \frac{V_r f_c}{k} \quad (138)$$

Since the target is moving with the radial velocity  $V_r$ , the target travels a distance of  $\Delta R$  in  $\Delta t = \Delta R/V_r$  seconds. Therefore, the range error  $\Delta R$  of Equation (138) results in a travel time  $\Delta t$  expressed as

$$\Delta t = \frac{f_c}{k} \quad (139)$$

Rihaczek states that as a result of Equation (139) the range indicated by the delay of the MF response peak corresponds to the range not at the time of signal impact but rather the range at time  $\Delta t$  later or earlier depending on the direction of the linear frequency sweep  $k$ . Therefore, the linear FM receiver provides a measure of extrapolated range  $R_e$ . The extrapolated range  $R_e$  for a positive slope  $k$  is measured  $\Delta t$  after signal impact and  $R_e$  for a negative slope  $k$  is measured  $\Delta t$  before signal impact (30:247-248). The measurement of extrapolated range  $R_e$  provides the means of accurately determining target range; otherwise, unambiguous range measurements with a chirp pulse compression receiver is limited to stationary targets.

The chirp pulse compression receiver can accurately extrapolate the range through the simple time translation  $\Delta t = f_c/k$  which is a constant of the radar even though the target DFS  $f_d$  is unknown. However, the receiver provides no means of accurately extrapolating the target velocity from a single pulse. When both target RTD and DFS are unknown, the chirp pulse compression receiver cannot simultaneously determine both the target parameters  $\tau_d$  and  $f_d$  from a single pulse. The target DFS  $f_d$  can be determined only from consecutive extrapolated range measurements

(30:249). Converting to range and radial velocity coordinates and assuming the target velocity does not significantly change between consecutive range measurements, the extrapolated target velocity can be expressed as

$$V_{re} = \frac{R_{e1} - R_{e2}}{T_p} \quad (140)$$

where  $R_{e1}$  and  $R_{e2}$  represent the consecutive extrapolated range measurements from two independently processed chirp pulses separated in time by  $T_p$ . At this point, the relevant issues of measuring the range and radial velocity of a single point target with a chirp pulse compression receiver have been discussed. This discussion provides an introduction to the topic of chirp pulse radar resolution which is the next topic presented.

For the case where numerous point targets are simultaneously imaged rather than a single point target, the resolution capability of the chirp pulse radar becomes the primary concern. Since the chirp pulse radar measures only extrapolated range with no capability of measuring radial velocity from a single pulse, point targets with the same extrapolated range cannot be resolved (30:251-252). The discussion with respect to Equations (136) and (137) showed that all point targets with combinations  $(\tau_d, f_d)$  which satisfy Equation (137) and thus lie along the central ridge of the chirp pulse ambiguity function will produce a MF peak at the same location  $\tau_p$  on the  $\tau$  axis. As a result, when multiple point targets have the RTD and DFS combinations which satisfy Equation (137), all the point target responses of the MF output sum together at  $\tau = \tau_p$  to form a single peak MF response at  $\tau_p$  which is inseparable. Therefore, in a dense target environment where the point targets are spread in both range and radial velocity, the degree of range resolution which the chirp pulse radar can achieve is a function of both the width of the MF response which is approximately  $1/B$  from Equation (135) and the width of the range and velocity "spread" of point targets which cause them to lie along the central ridge of the chirp pulse ambiguity function.

Consider a scenario where good range resolution is the primary requirement of the radar. Since range resolution performance of the chirp pulse radar is dependent upon the distribution in range and radial velocity of the point targets which compose the dense target environment, one can consider three cases of dense target. In each case the dense target is classified in terms of the velocity behavior of the point targets. For the first case, the point targets are stationary. For the second case, all the point targets move with the same radial velocity  $V_r$ . And finally for the third case, the point targets move with a mean radial velocity  $\bar{V}_r$  and move relative to each other. Each dense target case is discussed in the following paragraphs.

The first case is the easiest to analyze. Since all the point targets are stationary, no range-Doppler coupling occurs. For this case the scattering function  $S_{DR}\{\tau_d, f_d\}$  can be expressed as

$$S_{DR}\{\tau_d, f_d\} = S_{DR}\{\tau_d\}\delta(f_d) \quad (141)$$

Since only a single matched filter is employed for linear FM, the frequency variable  $f$  can be set to zero. Thus, the mean MFLSR response from Section 3.5 can be written as

$$E[|y(\tau, 0)|^2] = N_o + E_t \int \int_{-\infty}^{\infty} S_{DR}\{\tau_d, f_d\} \theta(\tau - \tau_d, -f_d) df_d d\tau_d \quad (142)$$

Substituting Equation (141) into Equation (142) yields

$$E[|y(\tau, 0)|^2] = N_o + E_t \int_{-\infty}^{\infty} S_{DR}\{\tau_d\} \theta(\tau - \tau_d, 0) d\tau_d \quad (143)$$

The form of Equation (143) shows that no coupling exists between the target range and Doppler frequency. Therefore, the dense stationary target is simply a range-spread target where the width of  $\theta(\tau - \tau_d, 0)$  across the  $\tau$  axis represents the width of the MF response in RTD  $\Delta\tau$ . The RTD resolution width  $\Delta\tau$  which the chirp pulse MFLSR can achieve is approximately  $1/B$ , and the range resolution width  $\Delta R$

is expressed as

$$\Delta R \simeq \frac{c}{2B} \quad (144)$$

Thus, the width of  $\theta(\tau - \tau_d, 0)$  across the  $\tau$  axis determines the range resolution of the chirp pulse radar.

Next, consider the second case where all the point targets move at the radial velocity  $V_r$  and are stationary with respect to each other. The scattering function  $S_{DR}\{\tau_d, f_d\}$  can be expressed as

$$S_{DR}\{\tau_d, f_d\} = S_{DR}\{\tau_d\} \delta(f_d - f_{dr}) \quad (145)$$

where  $f_{dr}$  is the DFS of the point targets due to the radial velocity  $V_r$ . Substitution of Equation (145) into the expression for the mean MFSLR response given in Equation (142) yields

$$E[|y(\tau, f)|^2] = N_o + E_t \int_{-\infty}^{\infty} S_{DR}\{\tau_d, f_{dr}\} \theta(\tau - \tau_d, -f_{dr}) d\tau_d \quad (146)$$

As in the first case, the form of Equation (146) shows that no coupling exists between the target range and Doppler frequency. If range extrapolation is employed, the width of  $\theta(\tau, f)$  across the  $\tau$  axis determines the range resolution width  $\Delta\tau$ . As in Case 1, the RTD resolution width  $\Delta\tau$  is approximately  $1/B$ , and the range resolution  $\Delta R$  is expressed as

$$\Delta R \simeq \frac{c}{2B} \quad (147)$$

In terms of velocity measurement, the method of velocity extrapolation as given in Equation (140) will not work here because the range is continuous, so the radar has no means of resolving with respect to velocity. Thus, the receiver provides no means of extrapolating the radial velocity  $V_r$  because the target is continuous in range.

And finally consider the third case where the point targets move with a mean velocity  $\bar{V}_r$ , and point target relative motion is nonzero. For the third case, range-

Doppler coupling in  $\bar{y}^2$  occurs. This third case represents the aerosol target environment which is consistent with the Shapiro aerosol scattering model given in Section 3.4. Due to the range-Doppler coupling associated with chirp signals and illustrated by the chirp ambiguity function of Figure 7, the degree of point target relative motion will determine the degree of range resolution which the chirp radar can achieve. A specific example in terms of Dr Shapiro's aerosol target model will provide a more quantitative description of the range resolution  $\Delta\tau$  which the chirp radar can achieve.

Dr. Shapiro has demonstrated the range resolution potential of a chirp pulse radar for aerosol imaging (33:1-5). Recall from Section 3.4 the Shapiro model of the aerosol target and from Section 3.5 the mean power MFSLR response. The mean power MFSLR response was expressed in general as

$$E [|y(\tau, f)|^2] = E \left[ \left| \int_{-\infty}^{\infty} r(t) s^*(t - \tau) \exp(-j2\pi ft) dt \right|^2 \right] \quad (148)$$

where  $r(t) = s_r(t) + n(t)$  and  $s_r(t)$  was expressed as

$$s_r(t) = E^{1/2} \int_{-\infty}^{\infty} s(t - \tau_d) \gamma_{DR}(\tau_d, t - \tau_d/2) d\tau_d \quad (149)$$

and  $\gamma_{DR}(\tau_d, t)$  which represents the Shapiro aerosol model was expressed as

$$\gamma_{DR}(\tau_d, t) = \exp(-j2\pi \bar{f}_d t) \int_{-\infty}^{\infty} T(\bar{\rho}, c\tau_d/2, t - \tau_d/2) \xi^2(\bar{\rho}, c\tau_d/2) d\bar{\rho} \quad (150)$$

To simplify the analysis, Dr Shapiro assumes that the mean Doppler frequency-shift (DFS)  $\bar{f}_d$  is equal to zero. Since the range can be extrapolated in the more general case where the mean DFS is nonzero, the simplification of setting the mean DFS to zero is not especially limiting. With this simplification, a single matched filter with  $f = 0$  is employed. Thus the mean power MFSLR response of Equation

(148) simplifies to

$$E [ |y(\tau, 0)|^2 ] = E \left[ \left| \int_{-\infty}^{\infty} r(t) s^*(t - \tau) dt \right|^2 \right] \quad (151)$$

Substituting Equation (149) and Equation (150) into Equation (151) yields an analytical expression for the mean power MFLSR response. The detailed calculations to determine the analytical expression of the mean power MFLSR response to an aerosol target are laborious and unnecessary for the present discussion of range resolution. Dr Shapiro's results are given without proof; however, Dr Shapiro's results were verified using the general model for the mean power MFLSR response with  $f = 0$ . Therefore, the mean MFLSR response of Equation (142) can be expressed as

$$E [ |y(\tau, 0)|^2 ] = N_o + E_t \int \int_{-\infty}^{\infty} S_{DR} \{ \tau_d, f_d \} \theta(\tau - \tau_d, -f_d) df_d d\tau_d \quad (152)$$

Recall that  $S_{DR} \{ \tau_d, f_d \}$  represents the PSD of the complex Gaussian random process  $\gamma_{DR}(\tau_d, t)$  of Equation (150) where  $\bar{f}_d = 0$ . Also recall from Section 3.4 the Shapiro aerosol model where  $S_{DR} \{ \tau_d, f_d \}$  is expressed as

$$S_{DR} \{ \tau_d, f_d \} = \frac{\lambda^2}{\pi^{1/2}} \beta \left( \frac{c\tau_d}{2} \right) \left| \xi \left( \mu, \frac{-\tau_d}{2} \right) \right|^4 t_c \exp \left( -\pi^2 t_c^2 f_d^2 \right) \quad (153)$$

Substituting Equation (153) into Equation (152) yields a general result for the mean power MFLSR response in terms of the Shapiro aerosol target model and the ambiguity function of the transmitted radar signal. Again, the detailed calculations are unnecessary. Either Equation (152) or Equation (151) yield the same expression for the mean MFLSR response for the aerosol target model. The results are stated as follows:

Dr Shapiro showed that transmission of a Gaussian chirp pulse expressed in complex baseband form as

$$s(t) = \left(\frac{8}{\pi T^2}\right)^{1/4} \exp \left[ -\left(\frac{4}{T^2} + j\pi k\right) t^2 \right] \quad (154)$$

will result in a mean power MFSLR response expressed in general form as

$$E[|y(\tau, 0)|^2] = \int_0^\infty Q(\tau_d) W(\tau - \tau_d) d\tau_d \quad (155)$$

where  $Q(\tau_d)$  is the infinite resolution, average aerosol backscatter profile, and where  $W(\tau - \tau_d)$  is a Gaussian range weighting function which determines the range resolution of the chirp pulse radar.  $W(\tau - \tau_d)$  can be expressed in general form as

$$W(\tau - \tau_d) = K \exp \left[ -\frac{8(\tau - \tau_d)^2}{\Delta\tau} \right] \quad (156)$$

where  $K$  is a system constant, and  $\Delta\tau$  is the full width in the  $\tau$  coordinate between the  $e^{-2}$  attenuation points of  $W(\tau - \tau_d)$ . Shapiro shows that  $\Delta\tau$  can be expressed as

$$\Delta\tau = \frac{2^{1/2}T}{\left[1 + (\pi BT/4)^2 / (1 + T^2/4t_c^2)\right]^{1/2}} \quad (157)$$

where  $T$  is the RMS time duration and  $B$  is the RMS bandwidth of the transmitted signal  $s(t)$ . Therefore,  $\Delta\tau$  represents the RTD resolution of the chirp pulse radar. Multiplying Equation (157) by  $c/2$  yields an analogous expression for the range resolution  $\Delta R$  given as

$$\Delta R = \frac{cT/2^{1/2}}{\left[1 + (\pi BT/4)^2 / (1 + T^2/4t_c^2)\right]^{1/2}} \quad (158)$$

For more details of the derivation, refer to Dr Shapiro's report (33:1-5).

The primary interest in terms of range resolution of chirp pulse radar is the nature of the range resolution  $\Delta R$  of Equation (158). Recall that the coherence

time  $t_c$  is a measure of the relative velocities of the aerosol particles. Therefore, as stated earlier, the degree of range resolution  $\Delta R$  which the chirp pulse radar achieves is a function of the distribution of aerosol radial velocities the lidar beam illuminates. When the point targets such as aerosols move relative to each other, the scattering function is broadened in frequency. As a result, the range resolution  $\Delta R$  is broadened to the extent of significant overlap of the chirp pulse ambiguity function  $\theta(\tau, f)$  and the scattering function  $S_{DR}\{\tau_d, f_d\}$  as illustrated in Figure 8. The schematic of Figure 8 is consistent with the results of Equations (158). Both show that  $\Delta R$  is a function of the volume distributions of  $\theta(\tau, f)$  and  $S_{DR}\{\tau_d, f_d\}$ .

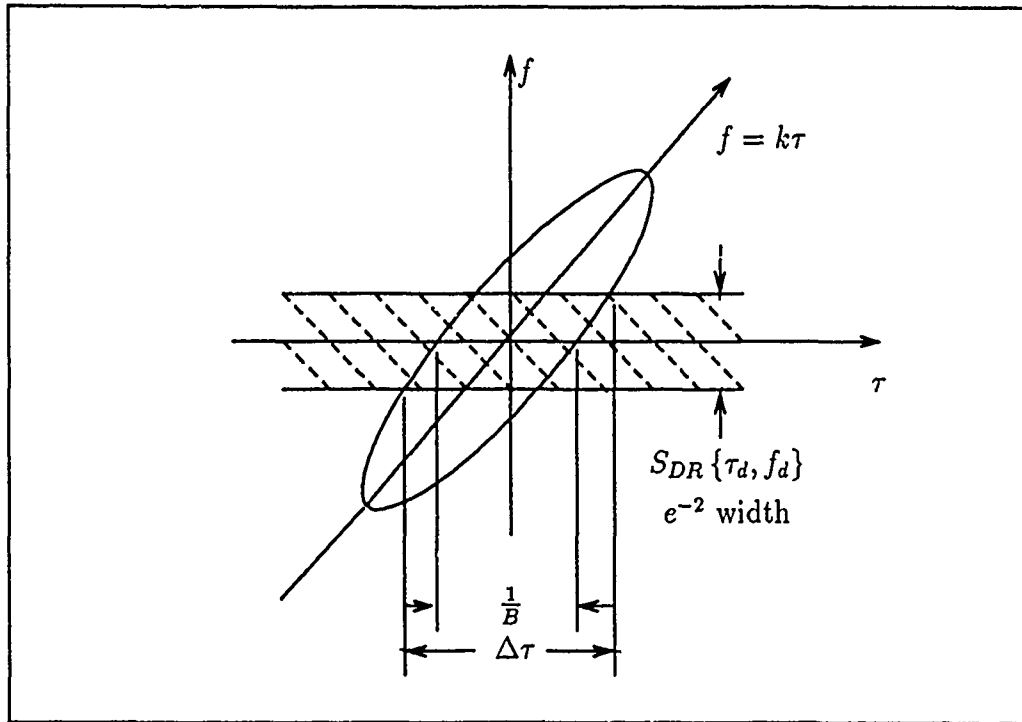


Figure 8. Combined Contour Plots of the Scattering and Ambiguity Functions

As an example, let  $T = 5\mu s$ ,  $t_c = 1\mu s$ , and  $B = 10MHz$ . Substitution into Equation (158) will yield  $\Delta R \simeq 72.6m$ . If the coherence time were extremely large which indicates minimal relative motion of aerosols,  $\Delta R \simeq 27m$ . Also in comparison



to an unmodulated pulse of the same time duration,  $\Delta R \simeq cT/2 \simeq 750m$ . It is clear from this example that with the assumption of a fixed mean velocity of aerosols, the relative velocity distribution of the aerosols somewhat degrades the pulse compression of the matched-filter but still improves range resolution performance compared to an unmodulated pulse of the same time duration. To achieve the same range resolution with the unmodulated pulse, the pulse duration  $T$  required is approximately equal to 0.5 microseconds. Due to transmitter peak power limitations, a  $5 \mu s$  pulse may reduce the maximum range of lidar operation. As in the second dense target case, no means of extrapolating the mean velocity is available since the target is continuous in range.

In summary, three cases of dense target have been considered, and for each case, a single linear FM matched-filter was employed. For Cases 1 and 2 where the point targets were assumed stationary with respect to each other, the width of  $\theta(\tau, 0)$  across the  $\tau$  axis determined the range resolution  $\Delta R$  of the chirp pulse radar. For Case 3, assuming  $\bar{f}_d = 0$  to simplify the analysis, relative motion of the point targets was included. As a result, the range resolution width  $\Delta R$  became a function of the volume distributions of both the scattering function  $S_{DR}\{\tau_d, f_d\}$  and the chirp pulse ambiguity function  $\theta(\tau, f)$ . For Cases 2 and 3 in general, the chirp pulse MFSLR could not extrapolate the mean velocity because the aerosol target was continuous in range.

To cover the topic of chirp pulse compression radar as thoroughly as possible, an additional approach for extrapolating target range and velocity of chirp pulses is presented. This second approach of chirp radar processing reported by Ramp and Wingrove (29:75-82) requires the transmission of two pulses of alternate linear FM slopes and corresponding matched-filters. Each signal is processed independently and combined to provide an interpretation of point target range and velocity. The basic signal processing for a single point target can be explained as follows: The transmission of a chirp pulse with positive slope  $k$  will result in a compressed pulse

MF response which peaks at

$$\tau_{(+)} = \tau_d - \Delta\tau_d \quad (159)$$

where  $\Delta\tau_d = f_d/|k|$ . Similarly, for a chirp pulse of negative slope  $k$ , the MF response peaks at

$$\tau_{(-)} = \tau_d + \Delta\tau_d \quad (160)$$

Therefore, the true target range-time delay  $\tau_d$  can be found by adding Equations (159) and (160) to obtain

$$\tau_d = \frac{\tau_{(+)} + \tau_{(-)}}{2} \quad (161)$$

Also, subtracting Equation (159) from Equation (160) and substituting  $\Delta\tau_d = f_d/|k|$  yields the expression for the DFS  $f_d$  given as

$$f_d = \frac{B}{T} \left( \frac{\tau_{(-)} - \tau_{(+)}}{2} \right) \quad (162)$$

Thus Equation (161) measures the target RTD and Equation (162) measures the target DFS. This type of signal processing described by Ramp and Wingrove has been demonstrated with a  $CO_2$  laser radar (16:152-162). While this type of receiver signal processing accurately determines the range and the velocity of a single point target without having to rely upon range extrapolation, this processing technique can determine neither range nor radial velocity of point targets in a dense target environment such as aerosols. As Rihaczek explains, with multiple point targets it will generally be impossible to order the received returns into their respective pairs to determine their combined range and radial velocity (30:251).

It has been shown that pulse compression radar will provide improved range resolution performance in terms of an aerosol target as a function of the degree of relative velocity of the aerosols at the expense of obtaining no velocity information. If the radar designer desires both range and velocity information of a target which consists of point targets distributed in range and velocity, the chirp pulse

does not offer a viable alternative to the simple unmodulated pulses designated as Class 1 radar signals. The remaining two classes of pulse compression radar signals to consider require less detailed analysis. The next case to consider is the large time-bandwidth product, pulse compression waveform which forms the thumbtack ambiguity function.

#### 4.4 Class 3 Radar Signals

A variety of signal waveforms often referred to as noise or pseudonoise waveforms with an ambiguity function shape which approximates the ambiguity diagram of Figure 9 are designated as Class 3 radar signals (38:418). This idealized ambiguity function is commonly referred to as the thumbtack ambiguity function in obvious reference to its shape. The approximate thumbtack ambiguity function of Figure 9 consists of a narrow central spike containing a negligibly small portion of the ambiguity volume. The nominal resolution cell is defined in terms of the central spike disjoint from the base of the ambiguity function and is expressed as

$$\Delta\tau\Delta f = \frac{1}{TB} \quad (163)$$

where  $T$  is the RMS time duration of the transmitted signal, and  $B$  is the RMS bandwidth of the transmitted signal. The volume of unity distributed across the area of dimensions  $T \times B$  with an approximate height of  $1/TB$  is called the pedestal of the ambiguity function. Large time-bandwidth product  $TB \gg 1$  waveforms which consist of long time-duration, large bandwidth signals generate the thumbtack ambiguity function. An infinite variety of signals referred to as noise waveforms such as signals obtained through random phase or frequency coding generate approximate thumbtack ambiguity functions. Another signal waveform which provides a poorer approximation to the thumbtack ambiguity function is waveforms with smoothly varying frequency modulation such as quadratic FM (31:505-507). More precise, three-dimensional ambiguity diagrams for various Class 3 waveforms may be found

in the radar literature (30).

As Rihaczek (30:133-140) and Siebert (35:219-220) explain, the narrowness of the central spike of the thumbtack ambiguity function provides excellent range and velocity resolution for the single target as long as the signal can be detected above the self clutter power interference. The self-clutter is obtained from contributions due to the point targets within the broad pedestal of dimensions  $T \times B$ . If the cross section of the target within the central spike of the ambiguity function is significantly stronger than the cumulative cross section of all the point targets within the pedestal of the ambiguity function, then the Class 3 waveform will provide improved resolution performance. To quantify this concept, radar texts usually introduce the term  $S/C$  for signal to clutter ratio.

Recall from Section 3.5 that the mean power MFSLR response is a two-dimensional convolution of the scattering function  $S_{DR}\{\tau_d, f_d\}$  with the ambiguity function  $\theta(\tau, f)$  which in this case is the thumbtack ambiguity function. The boundaries where  $S_{DR}\{\tau_d, f_d\}$  is significant (i.e.  $e^{-2}$  attenuation width) in the  $(\tau, f)$  plane defines the occupied target space. Since the scattering function is continuous in range, the range extent of the scattering function always extends beyond the dimension  $T$  of the pedestal across the  $\tau$  axis. If  $f_b$  is designated as the boundary where  $S_{DR}\{\tau_d, f_d\}$  is significant across the  $f$  axis, then either  $f_b < B$  or  $f_b > B$  where  $B$  is the dimension of the pedestal across the  $f$  axis. The analysis of the two cases where either  $f_b > B$  or  $f_b < B$  are briefly summarized from the Rihaczek text (30:133-140).

First consider the case where  $f_b > B$ . The desired nominal resolution cell is defined in terms of the widths across the  $\tau$  and  $f$  axes of the ambiguity function's central spike as in Equation (163). The pedestal surface of the ambiguity function can be divided by the area of the nominal resolution cell to determine the number  $N$  of resolution cells within the pedestal. Thus, the pedestal contains  $N$  nominal

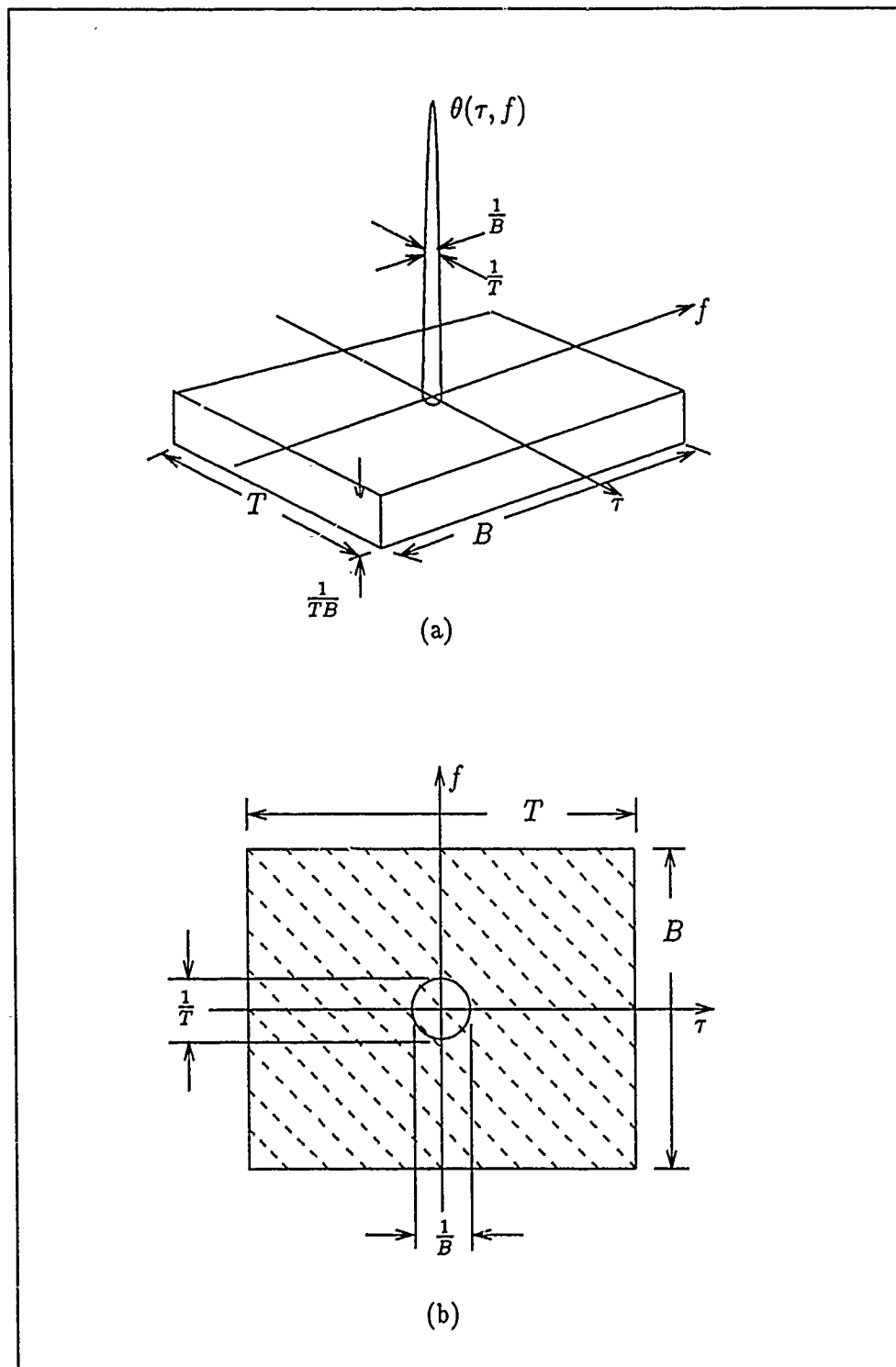


Figure 9. Class 3 Ambiguity Function (a) and Contour Plot (b) (35:217)

resolution cells where  $N$  is expressed as

$$N \simeq \frac{TB}{1/TB} \simeq (TB)^2 \quad (164)$$

Let  $\sigma$  represent the value of the scattering function within a resolution cell. If  $\sigma_c$  represents the cumulative cross section of the scattering function from each resolution cell, then the mean cross section of the scattering function in each cell can be expressed approximately as

$$\sigma_m = \frac{\sigma_c}{N} \quad (165)$$

Therefore, if  $\sigma_s$  represents the cross section value of the scattering function  $S_{DR}\{\tau_d, f_d\}$  at the resolution cell within the central spike of the ambiguity function, the average  $S/C$  can be expressed as

$$\frac{S}{C} \simeq \frac{\sigma_s(TB)}{\sigma_m N} \quad (166)$$

Substituting for  $N$  from Equation (164) into Equation (166) yields

$$\frac{S}{C} \simeq \left(\frac{1}{TB}\right) \left(\frac{\sigma_s}{\sigma_m}\right) \quad (167)$$

If the minimum signal to clutter ratio  $S/C$  is arbitrarily chosen as unity, then Equation (167) constrains the ratio  $\sigma_s/\sigma_m$  to

$$\frac{\sigma_s}{\sigma_m} \simeq TB \quad (168)$$

Equation (168) shows that to detect the signal with a minimum signal to clutter ratio of unity,  $\sigma_s$  must be  $TB$  greater than average. In other words, to achieve the resolution of the nominal resolution cell defined in Equation (163) with  $S/C = 1$ , the scattering function cross section  $\sigma_s$  must be  $TB$  higher than the average cross section level. Thus, any resolution cell of the scattering function for which  $\sigma_s < (TB \times \sigma_m)$

is completely masked in the self-clutter.

Next, consider the second case where  $f_b < B$ . For this case, resolution performance will improve somewhat. It is easily shown that when  $f_b < B$ , Equation (167) can be expressed as

$$\frac{S}{C} \simeq \left( \frac{1}{T f_b} \right) \left( \frac{\sigma_s}{\sigma_m} \right) \quad (169)$$

As in the first case, for a signal to clutter ratio of unity, Equation (169) can be expressed as

$$\frac{\sigma_s}{\sigma_m} \simeq T f_b \quad (170)$$

The form and interpretation of Equation (170) is analogous to that of Equation (168). To achieve the resolution of the nominal resolution cell defined in Equation (163) with  $S/C = 1$ , the scattering function cross section  $\sigma_s$  must be  $T f_b$  greater than average. Thus the resolution improves dependent upon the degree of significant overlap between  $f_b$  and  $B$ .

For either case, it is clear that the thumbtack ambiguity function does not achieve the desired resolution of the nominal resolution cell. In general, portions of the scattering function where  $\sigma_s$  is approximately less than or equal to the mean value  $\sigma_m$  are completely masked by the self-clutter; therefore, in a dense target environment, the true resolution which Class 3 signals achieve is defined by the broad dimensions of the ambiguity function pedestal. Rihaczek (30:133-140) shows that in general, the resolution of Class 3 signals in a dense target environment is inferior to the resolution of a simple unmodulated pulse designated as a Class 1 waveform. For these reasons, Rihaczek and Siebert state that the inferior resolution performance of Class 3 radar signals make them in general a poor choice of waveform in a dense target environment (30; 35). Therefore, Class 3 radar signals are not a viable option in comparison to Class 1 radar signals. The final radar signal to consider forms the so-called bed of nails ambiguity function.

#### 4.5 Class 4 Radar Signals

Class 4 radar signals form the so-called "bed of nails" ambiguity function. A uniformly-spaced coherent pulse train as in Figure 10 illustrates the common example of a Class 4 waveform. The periodic pulse train is essentially a means of producing a long time-duration signal for improved frequency resolution with a short time-duration pulse which provides good range resolution. If  $p(t)$  represents a single

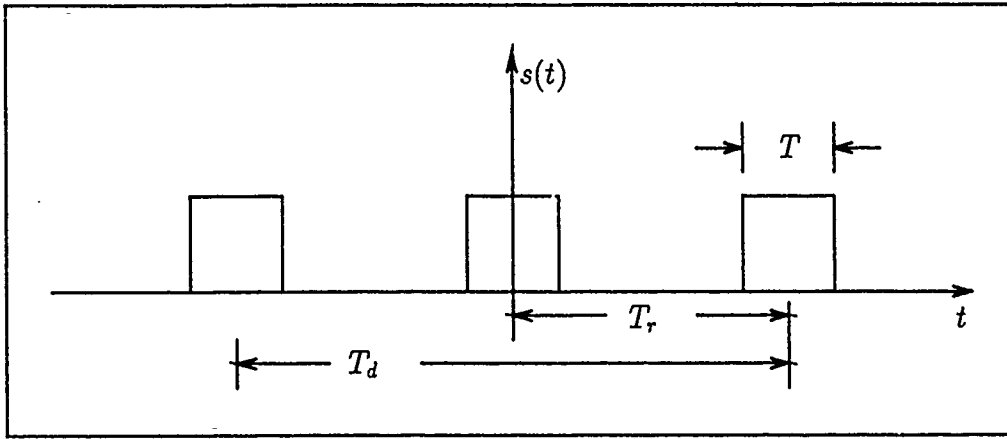


Figure 10. Periodic Pulse Train

complex pulse of duration  $T$  with the ambiguity function designated as  $\chi_p(\tau, f)$ , the complex periodic pulse train, normalized with respect to its energy can be expressed as

$$s(t) = \frac{1}{M^{1/2}} \sum_{m=0}^{M-1} p(t - mT_r) \quad (171)$$

where  $T_r$  is the pulse repetition period and  $M$  represents the total number of pulses. To simplify the analysis, the pulse train can be centered at time  $t = 0$  so that  $p(t)$  is expressed as

$$s(t) = \frac{1}{M^{1/2}} \sum_{m=0}^{M-1} p\left(t - mT_r + \frac{1}{2}(M-1)T_r\right) \quad (172)$$

The pulse train of Equation (172) is illustrated in Figure 10 for the common pulse duration of  $M = 3$ . Using Equation (172) to determine the ambiguity function,



Blahut (8:6-17-6-18) has shown that the ambiguity function can be expressed as

$$\chi(\tau, f) = \frac{1}{M} \sum_{m=-(M-1)}^{M-1} \chi_p(\tau - mT_r, f) \frac{\sin[\pi f T_r (M - |m|)]}{\sin(\pi f T_r)} \quad (173)$$

If it is assumed that the pulses are of short duration in comparison to the pulse repetition interval  $T_r$ , the components of the ambiguity function  $\chi_p(\tau, f)$  which are centered at  $\tau = mT_r$  will overlap only with their low sidelobe parts, so to a close approximation, one can look at each component ambiguity function individually. The component ambiguity function for one specific value of  $m$  can be written as

$$\chi_m(\tau, f) = \left[ \frac{M - |m|}{M} \right] \chi_p(\tau - mT_r, f) \left[ \frac{\sin \pi f (M - |m|) T_r}{(M - |m|) \sin \pi f T_r} \right] \quad (174)$$

The first term of Equation (174) within brackets forms a broad triangular envelope across the  $\tau$  axis. Within this triangular envelope, the ambiguity function  $\chi_p(\tau, f)$  is periodically repeated at each value of  $m$  across the  $\tau$  axis. Across the  $f$  axis,  $\chi_p$  forms a broad envelope, and the term

$$\frac{\sin \pi f (M - |m|) T_r}{\sin \pi f T_r} \quad (175)$$

samples the broad frequency envelope of  $\chi_p$  at  $f = k/T_r$  where  $k$  is an integer. The end result is an ambiguity function as illustrated in Figure 11 with fine structure both across the  $\tau$  axis and across the  $f$  axis (30:187).

To determine the nominal resolution cell dimensions in terms of the ambiguity function's central spike, the widths across each axis at the origin are measured according to any of the three resolution criteria. For RTD resolution, let  $m = 0$  and  $f = 0$  to simplify Equation (174) to

$$\chi_{m=0}(\tau, 0) = \chi_p(\tau, 0) \quad (176)$$

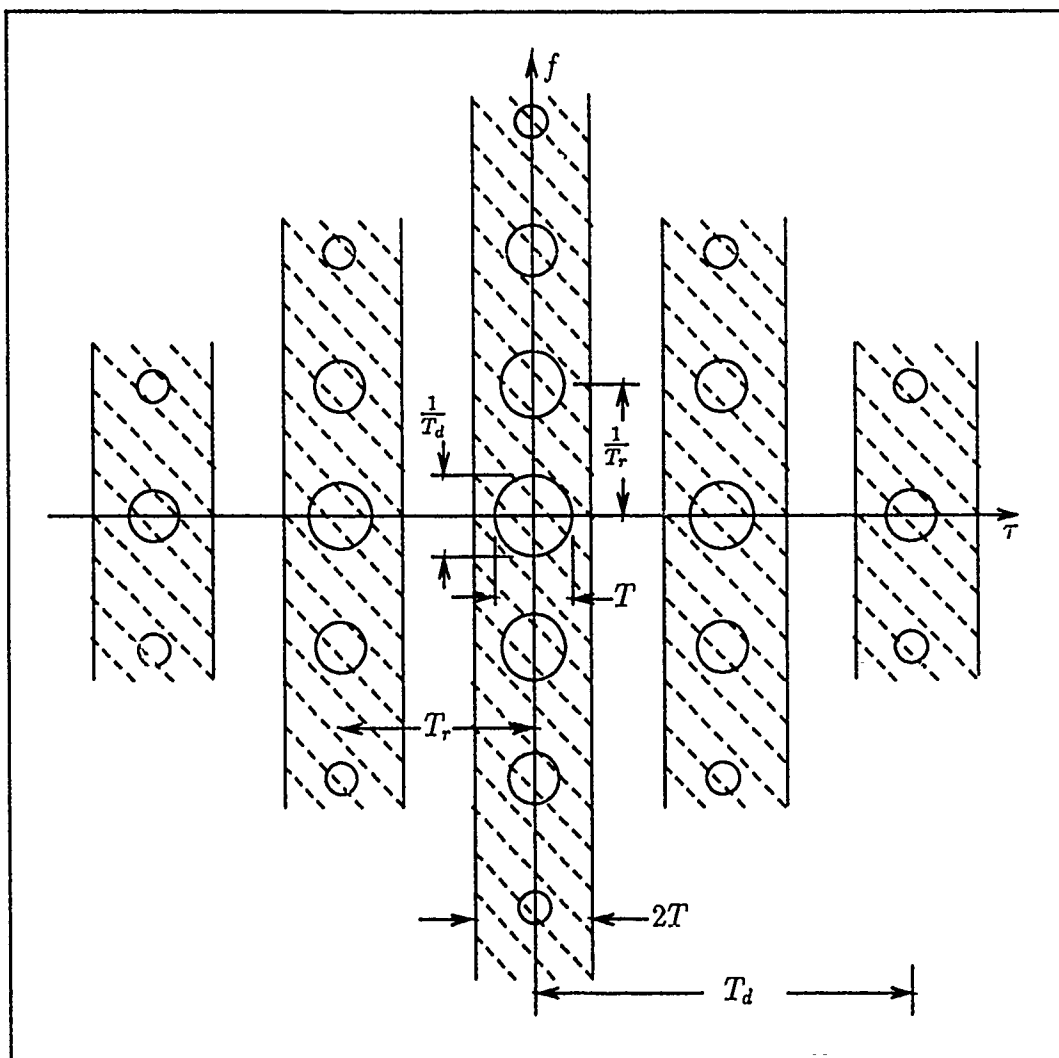


Figure 11. Contour Plot of a Class 4 Ambiguity Function (35:217)

which represents the ambiguity function across the  $\tau$  axis of a single pulse of duration  $T$ ; therefore, the RTD resolution width  $\Delta\tau \simeq T \simeq 1/B$  is the same as for a single pulse  $p(t)$  of duration  $T$  of the coherent pulse train. Similarly, to determine frequency resolution of the central spike across the  $f$  axis, let  $m = 0$  and  $\tau = 0$  so that

$$\chi_{m=0}(0, f) = \chi_p(0, f) \left[ \frac{\sin \pi f M T_r}{\sin \pi f T_r} \right] \quad (177)$$

The first null of Equation (177) occurs at  $f = 1/M T_r = 1/T_d$ ; therefore, the DFS resolution width can be written as

$$\Delta f = \frac{1}{M T_r} = \frac{1}{T_d} \quad (178)$$

The nominal time-frequency resolution cell is

$$\Delta\tau \Delta f \simeq \frac{1}{B T_d} \quad (179)$$

Range and radial velocity resolution widths can be expressed respectively as

$$\Delta R \simeq \frac{c}{2B} \quad (180)$$

$$\Delta V_r \simeq \frac{\lambda}{2T_d} \quad (181)$$

And therefore, the nominal range-velocity resolution cell can be expressed as

$$\Delta R \Delta V_r \simeq \frac{c\lambda}{4} \times \frac{1}{T_d B} \quad (182)$$

Thus, the coherent pulse train provides the range resolution of a single pulse of duration  $T$  and the improved velocity resolution of a single pulse of duration  $T_d$ . The cost of this improved resolution is range and velocity ambiguities as illustrated in Figure 11 where again the ambiguity function  $\theta(\tau, f)$  is approximated with a two-dimensional contour plot. Range ambiguities are seen to occur at multi-

ples of the pulse repetition interval  $T_r$  and frequency ambiguities are seen to occur at multiples of  $1/T_r$ . These range and frequency ambiguities are approximately of the same magnitude as the central spike; therefore, if targets are present beyond  $T_r$  in range or  $1/T_r$  in frequency, significant contributions from targets outside the nominal resolution cell will degrade resolution in either domain. Typically, coherent pulse trains are employed when the range and velocity extent of the target or targets of interest is confined to the immediate region surrounding the central spike of the ambiguity function as illustrated in Figure 12 (30:143). When the targets are confined to this region, the MFSLR response is of no interest beyond the value  $\tau_1$  corresponding to the outer limit of target range and  $f_1$  for target velocity. To create a large "clear" rectangular area about the central spike, one would logically desire that both range and velocity ambiguities are separated as much as possible. However, since the spread in range ambiguity is determined by  $T_r$  and the spread in velocity ambiguity is determined by  $1/T_r$ , a compromise between range ambiguity and velocity ambiguity is obviously required. The maximum unambiguous range is

$$R_m = \frac{cT_r}{2} \quad (183)$$

and the maximum unambiguous velocity is

$$V_m = \pm \frac{\lambda}{2T_d} \quad (184)$$

The product of the maximum unambiguous range and maximum unambiguous velocity is a constant of the radar expressed as

$$R_m V_m = \pm \frac{c\lambda}{4} \quad (185)$$

Equation (185) illustrates the trade-off required between maximum unambiguous range and maximum unambiguous velocity. This limitation is especially troublesome

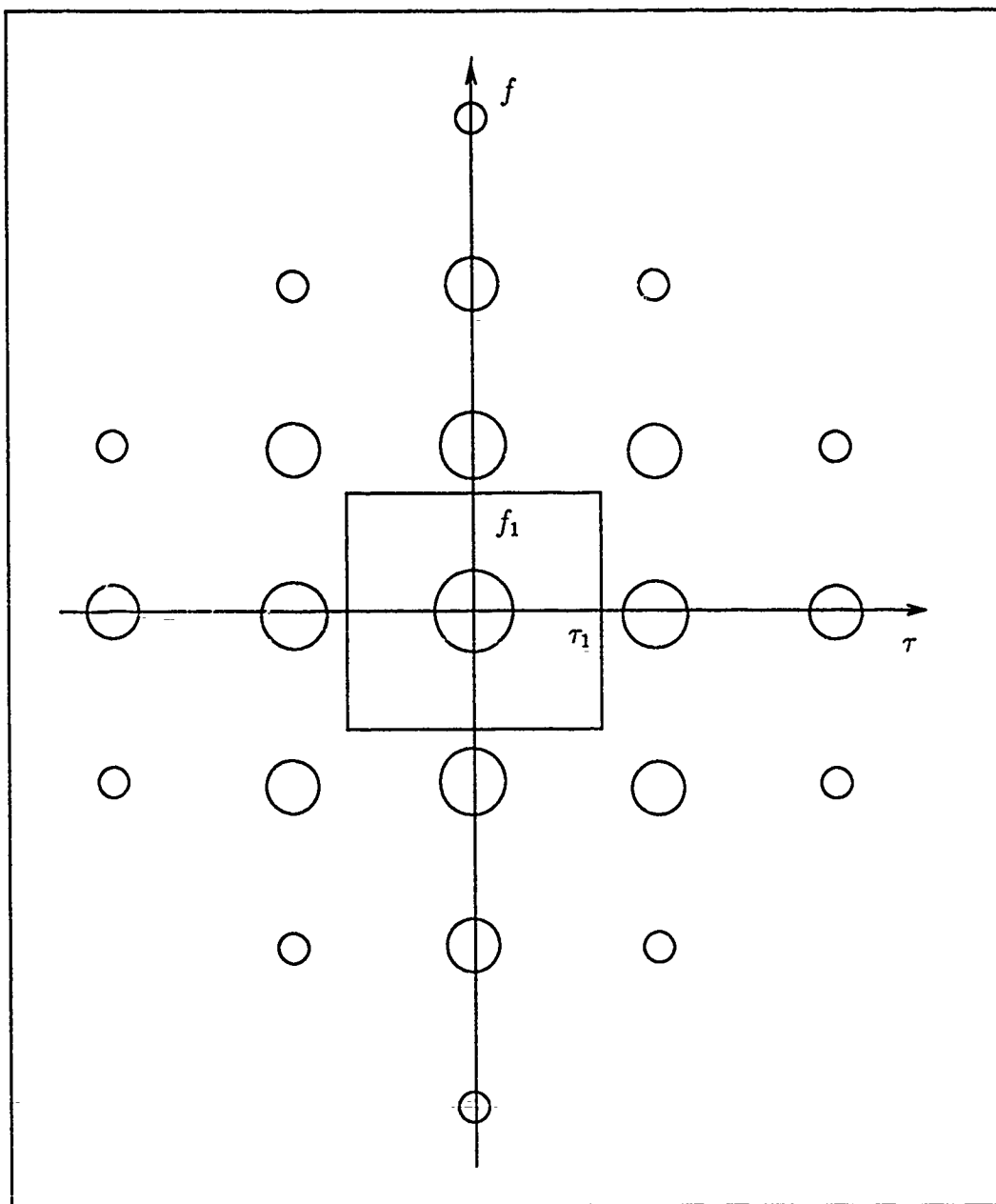


Figure 12. Clear Area about the Central Spike

for the atmospheric sensing lidar operating at a wavelength of  $10\mu m$ . Substituting  $\lambda = 10\mu m$  and  $c = 3 \times 10^8 m/s$  gives

$$R_m V_m = \pm 750 \frac{m^2}{s} \quad (186)$$

Equation (186) shows that the product  $R_m V_m$  is simply too small for most meteorological targets of interest using a  $CO_2$  lidar. For example, the CTI lidar with an aerosol range of approximately 5 kilometers will consist of velocity ambiguities beyond  $0.0375 m/s$ . Or conversely, the CTI lidar discussed in Section 2.4 can unambiguously detect aerosols of velocities from zero to  $\pm 35 m/s$ . For  $V_m = \pm 35 m/s$ ,  $R_m \simeq 21.4 m$ . These results show that for the case of aerosol imaging, coherent pulse trains are not in general a viable option for improving combined range and velocity resolution.

In summary, each of the four classes of radar signals have been evaluated with respect to their resolution capability. The ambiguity function for each class of waveform was evaluated in terms of the resolution with which the target scattering function  $S_{DR}\{\tau_d, f_d\}$  can be determined. The pulse compression waveforms designated as Classes 2, 3, and 4 were each compared to the resolution capability of the simple unmodulated pulse designated as a Class 1 radar signal. In each case, the pulse compression waveforms did not provide improved resolution performance in both range and radial velocity simultaneously. As a result, none of the pulse compression waveforms evaluated represent a viable alternative to the Class 1 radar signal currently in use in lidar systems.

## V. Conclusions and Recommendations

Results of this thesis effort provide a thorough review of conventional matched-filter radar theory as it applies to an aerosol sensing lidar. Chapter 2 provided an historical perspective of lidar development and a brief discussion of current lidar systems and signal processing techniques. Chapter 3 provided a discussion of the basic theory of conventional matched-filter radars, the complex aerosol target model, and the MFSLR response to the aerosol target model. The development of the MFSLR response given in Appendix A is considered to be an original result which provides the MFSLR response to any complex target satisfying the conditions of the Van Trees target model given in Section 3.4. In Chapter 4, each of the four classes of radar signals were evaluated in terms of their resolution performance. Each class of radar signal was evaluated in terms of the resolution with which it could reproduce the scattering function of the target.

### 5.1 Conclusions

As a result of this thesis effort, the mean MFSLR response to a dense, aerosol target environment can be expressed as

$$E[|y(\tau, f)|] = N_o + E_t \int \int_{-\infty}^{\infty} S_{DR}\{\tau_d, f_d\} \theta(\tau - \tau_d, f - f_d) d\tau_d df_d \quad (187)$$

where  $S_{DR}\{\tau_d, f_d\}$  represents the scattering function of the aerosol target or any complex target which satisfies the conditions of the Van Trees target model given in Section 3.4 and where  $\theta(\tau - \tau_d, f - f_d)$  represents the squared-modulus, matched-filter response to a single point target with range time-delay  $\tau_d$  and Doppler frequency-shift  $f_d$ . The MFSLR response derived in Appendix A represents a two-dimensional convolution of the target scattering function  $S_{DR}\{\tau_d, f_d\}$  with the signal ambiguity function  $\theta(\tau, f)$ . The resolution with which the MFSLR measures the scattering

function is dependent upon the volume distributions of both the ambiguity function and the aerosol scattering function. Since the normalized volume of  $\theta(\tau, f)$  is always fixed to equal unity, the four classes of radar waveforms are represented by ambiguity functions with different distributions of the same volume over the  $(\tau, f)$  plane. In each case, the waveform's resolution capability with respect to the target scattering function was evaluated. The pulse compression waveforms designated as Class 2, 3, and 4 radar signals did not provide an improved resolution capability in comparison to simple unmodulated pulses designated as Class 1 radar signals currently in use with aerosol sensing lidars. In conclusion, if a conventional MFSLR is employed, Class 1 radar signals represent the best choice in terms of resolution performance and receiver design simplicity.

## *5.2 Recommendations*

The question of whether more sophisticated pulse compression radar signals provide improved resolution performance with a conventional, matched-filter radar has been thoroughly researched, and the conclusion is that they do not. Class 1 radar signals represent the best choice signal for aerosol sensing lidars when a conventional, matched-filter receiver is employed. However, this thesis effort did not determine whether the MFSLR represents the optimum receiver design for a dense, aerosol target environment. It may be possible to make better use of the statistics of the aerosol target with a more sophisticated receiver design. The many receiver designs which Dr Van Trees develops in his text (39) may offer some insight into more sophisticated receiver designs to achieve better resolution performance.



## Appendix A. *Derivation of the MFSLR Response*

Consider the schematic of Figure 3 which illustrates an array of matched-filters followed by square-law envelope detectors. The mean power response of the MFSLR can be expressed analytically as

$$E [|y(\tau, f)|^2] = E \left[ \left| \int_{-\infty}^{\infty} [s_r(t) + n(t)] s^*(t - \tau) \exp(-j2\pi ft) dt \right|^2 \right] \quad (188)$$

Equation (188) can be written as

$$\begin{aligned} E [|y(\tau, f)|^2] &= \int \int_{-\infty}^{\infty} E \{ [s_r(t) + n(t)] [s_r^*(u) + n^*(u)] \} \\ &\quad \times [s^*(t - \tau) s(u - \tau)] \exp[-j2\pi f(t - u)] dt du \\ &= \int \int_{-\infty}^{\infty} E [s_r(t) s_r^*(u) + s_r(t) n^*(u) + s_r^*(u) n(t) + n(t) n^*(u)] \\ &\quad \times s^*(t - \tau) s(u - \tau) \exp[-j2\pi f(t - u)] dt du \end{aligned} \quad (189)$$

where  $n(t)$  is a zero-mean complex white Gaussian noise process due to the shot noise limited photodetector whose covariance function  $C_n(t, u)$  is expressed as

$$\begin{aligned} C_n(t, u) &= E [n(t) n^*(u)] \\ &= N_o \delta(t - u) \end{aligned} \quad (190)$$

where  $N_o$  is the spectral density  $h\nu/\eta$  of the photodetector shot noise limited, white Gaussian noise process. Taking the expected value of each term within brackets of Equation (189), the cross-terms  $E [s_r(t) n^*(u)]$  and  $E [s_r^*(u) n(t)]$  go to zero since  $n(t)$  is a zero-mean random process. Therefore, Equation (189) can be written as

$$\begin{aligned}
E[|y(\tau, f)|^2] &= \int \int_{-\infty}^{\infty} E[s_r(t)s_r^*(u)] s^*(t-\tau)s(u-\tau) \exp[-j2\pi f(t-u)] dt du \\
&\quad + \int \int_{-\infty}^{\infty} E[n(t)n^*(u)] s^*(t-\tau)s(u-\tau) \exp[-j2\pi f(t-u)] dt du
\end{aligned} \tag{191}$$

Substituting Equation (190) into Equation (191) and simplifying yields

$$E[|y(\tau, f)|^2] = N_o + \int \int_{-\infty}^{\infty} C_{s_r}(t, u) s^*(t-\tau)s(u-\tau) \exp[-j2\pi f(t-u)] dt du \tag{192}$$

where  $C_{s_r}$  is the complex covariance of the received signal expressed as

$$C_{s_r}(t, u) = E[s_r(t)s_r^*(u)] \tag{193}$$

and where  $s_r(t)$  has been normalized. Recall from the Van Trees model, the expression for the received signal given again as

$$s_r(t) = E_t^{1/2} \int_{-\infty}^{\infty} s(t-\tau_d) \gamma_{DR}(\tau_d, t - \frac{\tau_d}{2}) d\tau_d \tag{194}$$

where  $\gamma_{DR}(\tau_d, t)$  is a zero-mean complex Gaussian random process whose complex covariance  $C_\gamma(t, u)$  is expressed as

$$\begin{aligned}
C_\gamma(t, u) &= E[\gamma_{DR}(\tau_d, t) \gamma_{DR}^*(\tau_d', u)] \\
&= K_{DR}(\tau_d, t - u) \delta(\tau_d - \tau_d')
\end{aligned} \tag{195}$$

Substitution of Equation (194) into Equation (193) yields

$$C_{s_r}(t, u) = E_t \int \int_{-\infty}^{\infty} C_\gamma(t, u) s(t-\tau_d) s^*(u-\tau_d') d\tau_d d\tau_d' \tag{196}$$

Substituting Equation (195) into Equation (196) and simplifying yields

$$C_{sr}(t, u) = E_t \int_{-\infty}^{\infty} s(t - \tau_d) s^*(u - \tau_d) K_{DR}(\tau_d, t - u) d\tau_d \quad (197)$$

Recall from Section 3.4, the Fourier transform relation between  $K_{DR}(\tau_d, \alpha)$  of Equation (197) and the scattering function  $S_{DR}\{\tau_d, f_d\}$  expressed as

$$K_{DR}(\tau_d, \alpha) = \int_{-\infty}^{\infty} S_{DR}\{\tau_d, f_d\} \exp(j2\pi f_d \alpha) df_d \quad (198)$$

Substituting Equation (198) into Equation (197) yields

$$\begin{aligned} C_{sr}(t, u) = & E_t \int \int_{-\infty}^{\infty} s(t - \tau_d) s^*(u - \tau_d) S_{DR}\{\tau_d, f_d\} \\ & \times \exp[j2\pi f_d(t - u)] d\tau_d df_d \end{aligned} \quad (199)$$

Substituting Equation (199) into Equation (192) yields

$$\begin{aligned} E[|y(\tau, f)|^2] = & N_o + E_t \int \int_{-\infty}^{\infty} s^*(t - \tau) s(u - \tau) \exp[-j2\pi(f - f_d)(t - u)] \\ & \times \int \int_{-\infty}^{\infty} s(t - \tau_d) s^*(u - \tau_d) S_{DR}\{\tau_d, f_d\} d\tau_d df_d dt du \end{aligned} \quad (200)$$

Rearranging terms, Equation (200) can be expressed as

$$\begin{aligned} E[|y(\tau, f)|^2] = & N_o + E_t \int \int_{-\infty}^{\infty} S_{DR}\{\tau_d, f_d\} \\ & \times \int_{-\infty}^{\infty} s^*(t - \tau) s(t - \tau_d) \exp[-j2\pi(f - f_d)t] dt \\ & \times \int_{-\infty}^{\infty} s^*(u - \tau) s(u - \tau_d) \exp[-j2\pi(f - f_d)u] du d\tau_d df_d \\ = & N_o + E_t \int \int_{-\infty}^{\infty} S_{DR}\{\tau_d, f_d\} \\ & \times \int_{-\infty}^{\infty} s(t) s^*[t - (\tau - \tau_d)] \exp[-j2\pi(f - f_d)t] dt \end{aligned}$$

$$\times \int_{-\infty}^{\infty} s^*(u) s[u - (\tau - \tau_d)] \exp[j2\pi(f - f_d)u] du d\tau_d df_d \quad (201)$$

Recall the variable translations of Section 3.2 which led to the ambiguity function definition. The variable translations were

$$\tau' = \tau - \tau_d \quad (202)$$

$$f' = f - f_d \quad (203)$$

Substituting Equations (202) and (203) into Equation (201) yields

$$\begin{aligned} E[|y(\tau', f')|^2] &= N_c + E_t \int \int_{-\infty}^{\infty} S_{DR}\{\tau_d, f_d\} \\ &\quad \times \int_{-\infty}^{\infty} s(t) s^*(t - \tau') \exp(-j2\pi f' t) dt \\ &\quad \times \int_{-\infty}^{\infty} s^*(u) s(u - \tau') \exp(j2\pi f' u) du d\tau_d df_d \end{aligned} \quad (204)$$

Recall the ambiguity function definition given as

$$\chi(\tau, f) = \int_{-\infty}^{\infty} s(t) s^*(t - \tau) \exp(-j2\pi f t) dt \quad (205)$$

where the prime notation has been dropped for convenience. Thus, the squared modulus of  $\chi(\tau, f)$  designated as  $\theta(\tau, f)$  can be expressed as

$$\begin{aligned} \theta(\tau, f) &= |\chi(\tau, f)|^2 \\ &= \int_{-\infty}^{\infty} s(t) s^*(t - \tau) \exp(-j2\pi f t) dt \\ &\quad \times \int_{-\infty}^{\infty} s(u) s^*(u - \tau) \exp(j2\pi f u) du \end{aligned} \quad (206)$$

Substituting Equation (206) into Equation (204) yields the final expression for the MFSLR response given as

$$E [|y(\tau, f)|^2] = N_o + E_t \int \int_{-\infty}^{\infty} S_{DR} \{\tau_d, f_d\} \theta(\tau - \tau_d, f - f_d) d\tau_d df_d \quad (207)$$

Therefore, the mean power response of the MFSLR is in terms of the photodetector shot noise energy  $N_o$  and a two-dimensional convolution of the scattering function  $S_{DR} \{\tau_d, f_d\}$  with the radar signal ambiguity function  $\theta(\tau, f)$ . Equation (207) is useful for evaluating the MFSLR response in general for an arbitrary radar ambiguity function and arbitrary distributed target whose backscattered signal is described as a zero-mean, complex Gaussian random process.

## Bibliography

1. Bachman, C. G. *Laser Radar Systems and Techniques*. Dedham, Mass: Artech House, 1979.
2. Barnes, Norman P. and Charles E. Byvik. "Mid-Infrared Solid-State Lasers and Laser Materials," *Proceedings of SPIE Airborne and Spaceborne Lasers for Terrestrial Geophysical Sensing*, 889: 92-107. Bellingham, WA: SPIE, 1988.
3. Barton, David K. *Radars, Volume 3*. Dedham MA: Artech House, 1975.
4. Biernson, G. and R. F. Lucy. "Requirements of a Coherent Laser Pulse-Doppler Radar," *Proceedings of the IEEE*, 51: 202-213 (January 1963).
5. Bilbro, J. and others. "Airborne Doppler Lidar Wind Field Measurements," *Bulletin American Meteorological Society*, 65: 348-359 (April 1984).
6. Bilbro, James W. "Atmospheric laser Doppler velocimetry: an overview," *Optical Engineering*, 19: 533-542 (July 1980).
7. Bilbro, James W. and William W. Vaughn. "Wind Field Measurement in the Nonprecipitous Regions Surrounding Severe Storms by an Airborne Pulsed Doppler Lidar System," *Bulletin American Meteorological Society*, 59: 1095-1100 (September 1978).
8. Blahut, Richard E. *Theory of Remote Surveillance*. Reading MA: Addison-Wesley, 1988.
9. Byer, Robert L. "Diode Laser-Pumped Solid-State Lasers," *Science*, 239: 742-747 (February 1988).
10. Curran, Robert J. "Satellite-Borne Lidar Observations of the Earth: Requirements and Anticipated Capabilities," *Proceedings of the IEEE*, 77: 478-490 (March 1989).
11. Doviak, Richard J. and Dusan S. Zirnig. *Doppler Radar and Weather Observations*. Orlando FL: Academic Press, 1984.
12. Goodman, Joseph W. *Statistical Optics* New York: John Wiley and Sons, 1985.
13. Hardesty, R. Michael and others. "A ground-based, injection-locked, pulsed TEA laser for atmospheric wind measurements," *Proceedings of SPIE Airborne and Spaceborne Lasers for Terrestrial Geophysical Sensing*, 889: 23-28. Bellingham, WA: SPIE, 1988.
14. Hardesty, Michael R. *Measurement of Range-Resolved Water Vapor Concentration by Coherent CO<sub>2</sub> Differential Absorption Lidar*. PhD dissertation. Naval Postgraduate School, Monterey CA, 1984 (AD-A143 594).
15. Hardesty, Michael R., Senior Research Scientist. Telephone interview. NOAA Wave Propagation Laboratory, Boulder CO, 12 August 1990.

16. Henderson, D. M. and others. "Pulse Compression of an FM Chirped  $CO_2$  Laser," *Proceedings of SPIE Fifth Conference on Coherent Laser Radar: Technology and Applications*, 1181: 66-78. Bellingham, WA: SPIE, 1989.
17. Huffaker, R. M. and others. "Laser-Doppler System for Detection of Aircraft Trailing Vortices," *Proceedings of the IEEE*, 58: 322-326 (March 1970).
18. Huffaker, R. Milton. "Performance Analysis and Technical Assessment of Coherent Lidar Systems for Airborne Wind Shear Detection," *Proceedings of SPIE Airborne and Spaceborne Lasers for Terrestrial Geophysical Sensing*, 889: 65-76. Bellingham, WA: SPIE, 1988.
19. Kavaya, Michael J. and others. "Remote wind profiling with a solid-state Nd:YAG coherent lidar system," *Optics Letters*, 14: 776-778 (August 1989).
20. Kavaya, Michael J. and Robert T. Menzies. "Lidar aerosol backscatter measurements: systematic, modeling, and calibration error considerations," *Applied Optics*, 24: 3444-3453 (November 1985).
21. Klauder, J. R. "The Theory and Design of Chirp Radars," *The Bell System Technical Journal*, Vol. XXXIX No. 4: 745-808 (April 1960).
22. Lawrence, I. P. and R. M. Huffaker. "A Laser Velocimeter for Remote Wind Sensing," *The Review of Scientific Instruments*, 43: 512-518 (March 1972).
23. Lawrence, T. R. and others. "Feasibility and design considerations of a global wind sensing coherent infrared radar (WINDSAT)," *Proceedings of SPIE Physics and Technology of Coherent Infrared Radar*, 300: 34-43. Bellingham, WA: SPIE, 1981.
24. Menzies, Robert T. and R. Micheal Hardesty. "Coherent Doppler Lidar for Measurements of Wind Fields," *Proceedings of the IEEE*, 77: 449-462 (March 1989).
25. Menzies, Robert T., Senior Research Scientist. Telephone interview. Caltech Jet Propulsion Laboratory, Pasadena, CA, 10 July 1990.
26. Nathanson, Fred E. *Radar Design Principles*. New York: McGraw-Hill, 1969.
27. Petheram, J. F. and others. "The Laser Atmospheric Wind Sounder-Preliminary Design," *Proceedings of SPIE Fifth Conference on Coherent Laser Radar: Technology and Applications*, 1181: 66-78. Bellingham, WA: SPIE, 1989.
28. Post, M. J. and others. "National Oceanic and Atmospheric Administration's (NOAA) pulsed, coherent, infrared Doppler lidar - characteristics and data," *Proceedings of SPIE Fifth Conference on Coherent Laser Radar: Technology and Applications*, 300: 60-65. Bellingham, WA: SPIE, 1989.
29. Ramp, H. O. and E. R. Wingrove. "Principles of Pulse Compression," *IRE Transactions on Military Electronics*, MIL-5: 109-116 (April 1961).

30. Rihaczek, August W. *Principles of High-Resolution Radar*. New York: McGraw-Hill, 1969.
31. Rihaczek, August W. "Radar Waveform Selection - A Simplified Approach," *IEEE Transactions on Aerospace and Electronic Systems*, AES-7, No. 6: 1078-1086 (November 1971).
32. Schwiesow, R. L. and R. E. Cupp. "Remote Doppler velocity measurements of atmospheric dust devil vortices," *Applied Optics*, 15: 1-2 (January 1976).
33. Shapiro, Jeffrey H. *Coherent Laser Radar Remote Sensing, Appendix B*, Final Report, 19 January 1984. Massachusetts Institute of Technology, Lincoln Laboratory.
34. Siebert, William McC. "A Radar Detection Philosophy," *IRE Transactions on Information Theory*, IT-2, No. 3: 204-221 (September 1956).
35. Siebert, William McC. "A Radar Detection Philosophy," *IRE Transactions on Information Theory*, IT-2, No. 3: 204-221 (September 1956).
36. Sirmans, Dale and Bill Bumgarner. "Numerical Comparison of Five Mean Frequency Estimators," *Journal of Applied Meteorology*, 14: 991-1003 (September 1975).
37. Skolnik, Merrill I. *Radar Handbook*. New York: McGraw-Hill, 1970.
38. Skolnik, Merrill I. *Introduction to Radar Systems*. New York: McGraw-Hill, 1980.
39. Van Trees, Harry L. *Detection, Estimation, and Modulation Theory, Part III*. New York: John Wiley and Sons, 1971.
40. Wilson, David J. and others. "Laser Atmospheric Wind Sounder (LAWS) Technology Status," *Proceedings of SPIE Fifth Conference on Coherent Laser Radar: Technology and Applications*, 1181: 79-83. Bellingham, WA: SPIE, 1989.
41. Woodward, Philip M. *Probability and Information Theory, with Applications to Radar*. New York: McGraw-Hill, 1955.
42. Wright Research and Development Center, Air Force Systems Command. Contract F33615-88-C-1756 with Coherent Technologies Inc. Wright-Patterson AFB OH, 1 November 1989.



### *Vita*

Captain Jerry L. Rogers was born on 16 September 1959 in Bowdon, Georgia. He graduated from Bowdon High School in 1977 and married Rita N. Stewart. He graduated with honors from West Georgia College in 1982 earning a Bachelor of Arts degree in Mathematics. After teaching high school mathematics two years, he attended the USAF officer training school (OTS). He was commissioned in May 1984 and served his first tour as a student at Auburn University. He graduated with honors from Auburn in March 1986 with a Bachelor of Science degree in Electrical Engineering. Upon graduation, he served three years at Newark AFB, Ohio as a test equipment supervisor and inertial navigation systems engineer. He was selected in March 1989 to attend the School of Engineering, Air Force Institute of Technology.

Permanent address: 2057 Bonnie Dale Dr  
Bellbrook OH 45305

REPORT DOCUMENTATION PAGE			Form Approved OMB No. 0704-0188	
Public reporting burden for this collection of information is estimated to average 1 hour per response, including the time for reviewing instructions, searching existing data sources, gathering and maintaining the data needed, and completing and reviewing the collection of information. Send comments regarding this burden estimate or any other aspect of this collection of information, including suggestions for reducing this burden, to Washington Headquarters Services, Directorate for Information Operations and Reports, 1215 Jefferson Davis Highway, Suite 1204, Arlington, VA 22202-4302, and to the Office of Management and Budget, Paperwork Reduction Project (0704-0188), Washington, DC 20503.				
1. AGENCY USE ONLY (Leave blank)		2. REPORT DATE December 1990		3. REPORT TYPE AND DATES COVERED Master's Thesis
4. TITLE AND SUBTITLE Pulse Compression for Aerosol Ranging With Coherent Pulse-Doppler Lidar Systems			5. FUNDING NUMBERS	
6. AUTHOR(S) Jerry L. Rogers, Capt				
7. PERFORMING ORGANIZATION NAME(S) AND ADDRESS(ES) Air Force Institute of Technology, WPAFB OH 45433-6583			8. PERFORMING ORGANIZATION REPORT NUMBER AFTT/GE/ENG/90D-52	
9. SPONSORING/MONITORING AGENCY NAME(S) AND ADDRESS(ES) Electro-Optics WRDC/AARI-2 WPAFB OH 45433-6543			10. SPONSORING/MONITORING AGENCY REPORT NUMBER	
11. SUPPLEMENTARY NOTES				
12a. DISTRIBUTION / AVAILABILITY STATEMENT Approved for public release; distribution unlimited			12b. DISTRIBUTION CODE	
13. ABSTRACT (Maximum 200 words) <p>This thesis provides a thorough review of conventional matched filter radar theory as it applies to aerosol sensing lidar. Basic matched-filter radar theory and the complex, dense aerosol target model eventually lead to a general derivation of the matched-filter radar receiver response to a dense aerosol target environment. The matched-filter response is obtained in terms of a two dimensional convolution of the target scattering function and the radar ambiguity function. The range and radial velocity resolution of various radar signals were compared using the matched-filter radar receiver and scattering function models. Pulse compression radar signals were compared to the simple radar pulses currently in use with existing lidar systems, and in each case, the pulse compression radar signal did not provide a significant improvement in combined range and radial velocity resolution.</p> <p><i>Keywords: Theses,</i></p>				
14. SUBJECT TERMS Pulse Compression, Aerosol Ranging, Coherent Pulse-Doppler Lidar, Lidar Wind Sensing Systems, <del>Lidar</del> Laser Radar, (JH7) E			15. NUMBER OF PAGES 105	
			16. PRICE CODE	
17. SECURITY CLASSIFICATION OF REPORT Unclassified	18. SECURITY CLASSIFICATION OF THIS PAGE Unclassified	19. SECURITY CLASSIFICATION OF ABSTRACT Unclassified	20. LIMITATION OF ABSTRACT UL	